JOURNAL OF THE AERONAUTICAL SCIENCES

VOLUME 8 JUNE, 1941 NUMBER 8

The Buckling of Thin Cylindrical Shells under Axial Compression

THEODORE VON KÁRMÁN AND HSUE-SHEN TSIEN

California Institute of Technology

IN TWO PREVIOUS papers[1, 2] the authors have discussed in detail the inadequacy of the classical theory of thin shells in explaining the buckling phenomenon of cylindrical and spherical shells. It was shown that not only the calculated buckling load is 3 to 5 times higher than that found by experiments, but the observed wave pattern of the buckled shell is also different from that predicted. Furthermore, it was pointed out that the different explanations for this discrepancy advanced by L. H. Donnell[3] and W. Flügge[4] are untenable when certain conclusions drawn from these explanations are compared with the experimental facts. By a theoretical investigation on spherical shells[1] the authors were led to the belief that in general the buckling phenomenon of curved shells can only be explained by means of a non-linear large deflection theory. This point of view was substantiated by model experiments on slender columns with non-linear elastic support.[2] The non-linear characteristics of such structures cause the load necessary to keep the shell in equilibrium to drop very rapidly with increase in wave amplitude once the structure started to buckle. Thus, first of all, a part of the elastic energy stored in the shell is released once the buckling has started; this explains the observed rapidity of the buckling process. Furthermore, as it was shown in one of the previous papers[2] the buckling load itself can be materially reduced by slight imperfections in the test specimen and vibrations during the testing process.

In this paper, the same ideas are applied to the case of a thin uniform cylindrical shell under axial compression. First it is shown by an approximate calculation that again the load sustained by the shell drops with increasing deflection. Then the results of this calculation are used for a more detailed discussion of the buckling process as observed in an actual testing machine.

Received February 1, 1941.

Stresses in the Median Surface and the Expression for the Total Energy of the System

Let x and y be measured in the axial and the circumferential direction in the median surface of the undeformed cylindrical shell and u, v and w be the components of displacement of a point on the median surface of the shell in the x-direction, the y-direction and the radial direction (Fig. 1). Then at an arbitrary point in the median surface the unit strains in the x and y-directions, ϵ_x, ϵ_y and the unit shear γ_{xy} can be expressed in the following forms, including terms up to second order:

$$\begin{aligned} \epsilon_x &= \frac{\partial u}{\partial x} + \frac{1}{2}\left(\frac{\partial w}{\partial x}\right)^2 \\ \epsilon_y &= \frac{\partial v}{\partial y} + \frac{1}{2}\left(\frac{\partial w}{\partial y}\right)^2 - \frac{w}{R} \\ \gamma_{xy} &= \frac{\partial u}{\partial y} + \frac{\partial v}{\partial x} + \frac{\partial w}{\partial x}\frac{\partial w}{\partial y} \end{aligned} \tag{1}$$

R is the radius of the undeformed median surface of the shell. The stresses and the strains in the median surface of the shell are, however, related to each other by the following equations:

$$\begin{aligned} \sigma_x &= \frac{E}{1-\nu^2}(\epsilon_x + \nu\epsilon_y) \\ \sigma_y &= \frac{E}{1-\nu^2}(\epsilon_y + \nu\epsilon_x) \\ \tau_{xy} &= \frac{E}{2(1+\nu)}\gamma_{xy} \end{aligned} \tag{2}$$

where E is Young's modulus of elasticity and ν is Poisson's ratio. Therefore, by substituting Eq. (1) into Eq. (2), the following connections between the components of stress in the median surface and the

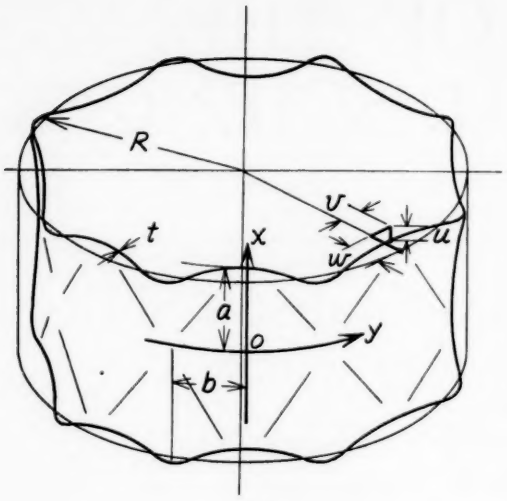

FIG. 1.

components of displacement of the median surface are obtained:

$$\sigma_x = \frac{E}{1-\nu^2}\left[\frac{\partial u}{\partial x} + \frac{1}{2}\left(\frac{\partial w}{\partial x}\right)^2 + \nu\left\{\frac{\partial v}{\partial y} + \frac{1}{2}\left(\frac{\partial w}{\partial y}\right)^2 - \frac{w}{R}\right\}\right]$$

$$\sigma_y = \frac{E}{1-\nu^2}\left[\frac{\partial v}{\partial y} + \frac{1}{2}\left(\frac{\partial w}{\partial y}\right)^2 - \frac{w}{R} + \nu\left\{\frac{\partial u}{\partial x} + \frac{1}{2}\left(\frac{\partial w}{\partial y}\right)^2\right\}\right] \quad (3)$$

$$\tau_{xy} = \frac{E}{2(1+\nu)}\left[\frac{\partial u}{\partial y} + \frac{\partial v}{\partial x} + \frac{\partial w}{\partial x}\frac{\partial w}{\partial y}\right]$$

It is generally accepted that the conditions of equilibrium between the stresses acting in the median surface of a thin shell can be approximately expressed by the equations used for flat plates:

$$\frac{\partial \sigma_x}{\partial x} + \frac{\partial \tau_{xy}}{\partial y} = 0$$
$$\frac{\partial \tau_{xy}}{\partial x} + \frac{\partial \sigma_y}{\partial y} = 0 \quad (4)$$

This pair of equations can be satisfied by introducing the well known Airy's stress function, $F(x, y)$, defined by the relations

$$\sigma_x = \frac{\partial^2 F}{\partial y^2}, \quad \tau_{xy} = -\frac{\partial^2 F}{\partial x \partial y}, \quad \sigma_y = \frac{\partial^2 F}{\partial x^2} \quad (5)$$

Eliminating the variables u and v in Eqs. (3) and (5) the following relation between Airy's stress function $F(x, y)$ and the radial component of the displacement, w is obtained:

$$\left(\frac{\partial^2}{\partial x^2} + \frac{\partial^2}{\partial y^2}\right)^2 F = E\left[\left(\frac{\partial^2 w}{\partial x \partial y}\right)^2 - \frac{\partial^2 w}{\partial x^2}\frac{\partial^2 w}{\partial y^2} - \frac{1}{R}\frac{\partial^2 w}{\partial x^2}\right] \quad (6)$$

This equation expresses the condition of compatibility between stress and strain. When $R \to \infty$, it reduces to the corresponding equation for a flat plate derived by the senior author.[5] L. H. Donnell[3] first obtained Eq. (6) in its present form. With a given distribution of the radial component of the displacement, w, Eq. (6) gives the induced stresses in the median surface of the shell.

For one complete wave panel, the extensional elastic energy W_1 corresponding to these stresses can be written as

$$W_1 = \frac{t}{2E} 4 \int_0^a \int_0^b [(\sigma_x + \sigma_y)^2 - 2(1+\nu)(\sigma_x\sigma_y - \tau_{xy}^2)]d\alpha\, dy \quad (7)$$

where a and b are the half wave lengths in the axial and the circumferential directions, respectively.

To calculate the elastic energy of bending, it is necessary to find the expressions for the change of curvatures and the unit twist of the median surface. In this paper, the following simplified expressions will be used:

$$\chi_x = \frac{\partial^2 w}{\partial x^2}, \quad \chi_{xy} = \frac{\partial^2 w}{\partial x \partial y}, \quad \chi_y = \frac{\partial^2 w}{\partial y^2} \quad (8)$$

In Eq. (8), certain additional terms in χ_y and χ_{xy} involving v are neglected. It was shown by L. H. Donnell[6] that if the terms retained in Eq. (8) are considered as of the order one, the neglected terms are of the order $1/n^2$, where n is the number of waves in the circumferential direction. For thin cylindrical shells, the value of n is around 10; therefore the neglection is justified. With these expressions for the change of curvatures and the unit twist of the median surface, the bending energy W_2 for one complete wave panel can be written as

$$W_2 = \frac{t^3 E}{24(1-\nu^2)} 4 \int_0^a \int^b \left[\left\{\frac{\partial^2 w}{\partial x^2} + \frac{\partial^2 w}{\partial y^2}\right\}^2 - 2(1-\nu)\left\{\frac{\partial^2 w}{\partial x^2}\frac{\partial^2 w}{\partial y^2} - \left(\frac{\partial^2 w}{\partial x \partial y}\right)^2\right\}\right] dx\, dy \quad (9)$$

The virtual work of the force applied on the end of the cylindrical shell can be calculated as the product of the applied force and the change in length of the shell. Therefore the following expression is obtained for one complete wave panel:

$$W_3 = 4t \int_0^b (\sigma_x)_{x=a}\, dy \int_0^a \frac{\partial u}{\partial x}\, dx \quad (10)$$

The equilibrium condition of the shell can be obtained either by equating the first variation of the difference between the sum of the energies W_1 and W_2

and the virtual work W_3 to zero, or by actually analyzing the moments and the stresses in the median surface of the shell. Using the approximations stated previously, Donnell[6] derived the equilibrium equation as

$$\frac{Et^3}{12(1-\nu^2)}\left(\frac{\partial^2}{\partial x^2}+\frac{\partial^2}{\partial y^2}\right)^4 w+\frac{Et}{R^2}\frac{\partial^4 w}{\partial x^4}= \left(\frac{\partial^2}{\partial x^2}+\frac{\partial^2}{\partial y^2}\right)^2\left\{p+t\left(\sigma_x\frac{\partial^2 w}{\partial x^2}+2\tau_{xy}\frac{\partial^2 w}{\partial x\,\partial y}+\sigma_y\frac{\partial^2 w}{\partial x^2}\right)\right\} \quad (11)$$

where p is the external radial pressure on the surface of the shell. In the case concerned, $p = 0$, then using Eq. (5), the second equation connecting Airy's stress function $F(x, y)$ and the radial component of displacement w is obtained as

$$\frac{Et^2}{12(1-\nu^2)}\left(\frac{\partial^2}{\partial x^2}+\frac{\partial^2}{\partial y^2}\right)^4 w+\frac{E}{R^2}\frac{\partial^4 w}{\partial x^4}= \left(\frac{\partial^2}{\partial x^2}+\frac{\partial^2}{\partial y^2}\right)^2\left[\frac{\partial^2 F}{\partial y^2}\frac{\partial^2 w}{\partial x^2}-2\frac{\partial^2 F}{\partial x\,\partial y}\frac{\partial^2 w}{\partial x\,\partial y}+\frac{\partial^2 F}{\partial x^2}\frac{\partial^2 w}{\partial y^2}\right] \quad (12)$$

When $R \to \infty$, Eq. (12) reduces to the corresponding equation for a flat plate.

There are two different ways to solve the problem of buckling of a thin uniform cylindrical shell under axial compression. The more exact method is to solve Eqs. (6) and (12) simultaneously, using appropriate boundary conditions. The approximate method is to first assume a plausible function for w, with undetermined parameters and then use Eq. (6) to determine the stresses in the median surface of the shell. The expressions W_1, W_2 and W_3 can then be calculated by means of Eqs. (7), (9) and (10). The undetermined parameters can be ascertained by the condition that $W_1 + W_2 - W_3$ must be a minimum. This approximate method will be used in the following calculations.

Calculation of the Total Energy

To obtain a plausible form for w, one has to resort to the experimental results. It is observed that, for large values of the wave amplitude, the waves show a so-called diamond shaped pattern. This particular wave shape can be approximately expressed by

$$\frac{w_1}{R}=\cos^2\frac{(mx+ny)}{2R}\cos^2\frac{(mx-ny)}{2R} \quad (13)$$

where the squares are introduced to account for the fact that the shell has a definite preference to buckle inward. Eq. (13) can be re-written as

$$\frac{w_1}{R}=\frac{1}{4}+\frac{1}{2}\left[\cos\frac{mx}{R}\cos\frac{ny}{R}+\frac{1}{4}\cos\frac{2mx}{R}+\frac{1}{4}\cos\frac{2ny}{R}\right] \quad (14)$$

On the other hand, the classical theory which is correct for infinitesimal values of the wave amplitude requires the wave to be of the form

$$\frac{w_2}{R}=\cos\frac{mx}{R}\cos\frac{ny}{R} \quad (15)$$

In order to satisfy this requirement, the wave form assumed in the following calculation is

$$\frac{w}{R}=\left(f_0+\frac{f_1}{4}\right)+\frac{f_1}{2}\left(\cos\frac{mx}{R}\cos\frac{ny}{R}+\frac{1}{4}\cos\frac{2mx}{R}+\frac{1}{4}\cos\frac{2ny}{R}\right)+\frac{f_2}{4}\left(\cos\frac{2mx}{R}+\cos\frac{2ny}{R}\right) \quad (16)$$

where f_0, f_1, f_2 are unknowns to be determined by the minimum condition given above; f_0 is introduced in order to allow the shell to expand radially. The amplitude of the wave pattern defined as the maximum difference in the radial deflection w is evidently given by f_1. The wave lengths in the axial and the circumferential direction are $2\pi R/m$ and $2\pi R/n$, respectively. Hence the number of waves along the circumference of the shell is equal to n. It is evident that no end effect can be accounted for by this form of wave pattern, and therefore the following calculation really corresponds to the case of a very long cylindrical shell. This simplification is justified by the experimental findings of N. Nojima and S. Kanemitsu as reported in a previous paper.[2] It was found that there is no appreciable length effect when the length of the cylindrical is greater than 1.5 times the radius of the shell. Furthermore, it is seen that by setting $f_0 = f_2 = 0$, Eq. (16) is reduced to Eq. (14); while by setting $(f_1/4) + (f_2/2) = 0$ and $f_0 + f_1/4 = 0$, Eq. (16) is reduced to Eq. (15). With other values of these parameters, wave patterns intermediate between these two limits can be obtained.

Substituting Eq. (16) into Eq. (6), the differential equation for Airy's stress function $F(x, y)$ is obtained:

$$\left(\frac{\partial^2}{\partial x^2}+\frac{\partial^2}{\partial y^2}\right)^2 F=-E\mu^2\left(\frac{n}{R}\right)^2\left[A\cos\frac{2mx}{R}+B\cos\frac{2ny}{R}+C\cos\frac{mx}{R}\cos\frac{ny}{R}+D\cos\frac{3mx}{R}\cos\frac{ny}{R}+G\cos\frac{mx}{R}\cos\frac{3ny}{R}+H\cos\frac{2mx}{R}\cos\frac{2ny}{R}\right] \quad (17)$$

where $\mu = m/n$, the "aspect ratio" of the waves. If $\mu > 1$, the waves are longer in the circumferential direction; if $\mu < 1$, the waves are longer in the axial direction. The coefficients in Eq. (17) are given by the following relations:

$$A=\frac{1}{8}f_1^2n^2-\left(\frac{1}{2}f_1+f_2\right)$$

$$B=\frac{1}{8}f_1^2n^2$$

$$C = \frac{1}{2}f_1n^2\left(\frac{1}{2}f_1 + f_2\right) - \frac{1}{2}f_1$$

$$D = \frac{1}{4}f_1n^2\left(\frac{1}{2}f_1 + f_2\right)$$

$$G = \frac{1}{4}f_1n^2\left(\frac{1}{2}f_1 + f_2\right)$$

and

$$H = n^2\left(\frac{1}{2}f_1 + f_2\right)^2 \tag{18}$$

The solution of Eq. (17) can be easily obtained as

$$F = -E\mu^2\left(\frac{R}{n}\right)^2\left[\frac{A}{16\mu^4}\cos\frac{2mx}{R} + \frac{B}{16}\cos\frac{2ny}{R} + \frac{C}{(1+\mu^2)^2}\cos\frac{mx}{R}\cos\frac{ny}{R} + \frac{D}{(1+9\mu^2)^2}\cos\frac{3mx}{R}\cos\frac{ny}{R} + \frac{G}{(9+\mu^2)^2}\times\cos\frac{mx}{R}\cos\frac{3ny}{R} + \frac{H}{16(1+\mu^2)^2}\cos\frac{2mx}{R}\times\cos\frac{2ny}{R}\right] + \frac{\alpha x^2}{2} + \frac{\beta y^2}{2} \tag{19}$$

Using Eq. (5), the stress components in the median surface can be written as

$$\sigma_x = E\mu^2\left[\frac{B}{4}\cos\frac{2ny}{R} + \frac{C}{(1+\mu^2)^2}\cos\frac{mx}{R}\cos\frac{ny}{R} + \frac{D}{(1+9\mu^2)^2}\cos\frac{3mx}{R}\cos\frac{ny}{R} + \frac{9G}{(9+\mu^2)^2}\cos\frac{mx}{R}\times\cos\frac{3ny}{R} + \frac{H}{4(1+\mu^2)^2}\cos\frac{2mx}{R}\cos\frac{2ny}{R}\right] + \beta$$

$$\sigma_y = E\mu^2\left[\frac{A}{4\mu^2}\cos\frac{2mx}{R} + \frac{\mu^2C}{(1+\mu^2)^2}\cos\frac{mx}{R}\cos\frac{ny}{R} + \frac{9\mu^2}{(1+9\mu^2)^2}\cos\frac{3mx}{R}\cos\frac{ny}{R} + \frac{\mu^2G}{(9+\mu^2)^2}\cos\frac{mx}{R}\times\cos\frac{3ny}{R} + \frac{\mu^2H}{4(1+\mu^2)^2}\cos\frac{2mx}{R}\cos\frac{2ny}{R}\right] + \alpha\times$$

$$t_{xy} = E\mu^2\left[\frac{\mu C}{(1+\mu^2)^2}\sin\frac{mx}{R}\sin\frac{ny}{R} + \frac{3\mu D}{(1+9\mu^2)^2}\sin\frac{3mx}{R}\sin\frac{ny}{R} + \frac{3\mu G}{(9+\mu^2)^2}\sin\frac{mx}{R}\sin\frac{3ny}{R} + \frac{\mu H}{4(1+\mu^2)^2}\sin\frac{2mx}{R}\sin\frac{2ny}{R}\right] \tag{20}$$

In all experimental work, the data are usually expressed in terms of the average compression stress σ in the axial direction. It can be easily seen from Eq. (20) that

$$\beta = -\sigma \tag{21}$$

Using Eq. (3), the following expressions for $\partial u/\partial x$ and $\partial v/\partial y$ can be obtained:

$$\frac{\partial u}{\partial x} = \frac{1}{E}(\sigma_x - \nu\sigma_y) - \frac{1}{2}\left(\frac{\partial w}{\partial x}\right)^2$$

$$\frac{\partial v}{\partial y} = \frac{1}{E}(\sigma_y - \nu\sigma_x) - \frac{1}{2}\left(\frac{\partial w}{\partial y}\right)^2 + \frac{w}{R} \tag{22}$$

By substituting Eqs. (16) and (20) into Eq. (22), it is found that

$$\frac{\partial u}{\partial x} = -\left[\left(\frac{\sigma}{E} + \nu\frac{\alpha}{E}\right) + \frac{1}{2}n^2\mu^2\left(\frac{3}{32}f_1^2 + \frac{1}{8}f_1f_2 + \frac{1}{8}f_2^2\right)\right] + \text{Terms of periodic functions} \tag{23}$$

$$\frac{\partial v}{\partial y} = \frac{\alpha}{E} + \nu\frac{\sigma}{E} - \frac{1}{2}n^2\left(\frac{3}{32}f_1^2 + \frac{1}{8}f_1f_2 + \frac{1}{8}f_2^2\right) + \left(f_0 + \frac{f_1}{4}\right) + \text{Terms of periodic functions}$$

Since y is measured along the circumference of the shell, v must be a periodic function of y; therefore, the constant term in $\dfrac{\partial v}{\partial y}$ must be equal to zero. Or

$$\frac{\alpha}{E} + \nu\frac{\sigma}{E} - \frac{1}{2}n^2\left(\frac{3}{32}f_1^2 + \frac{1}{8}f_1f_2 + \frac{1}{8}f_2^2\right) + \left(f_0 + \frac{f_1}{4}\right) = 0 \tag{24}$$

This condition determines α.

Using Eqs. (7), (20) and (24), the extensional energy W_1 of the shell is obtained as

$$\frac{W_1}{\frac{1}{2}Etab} = 4\left[(1-\nu^2)\left(\frac{\sigma}{E}\right)^2 + n^4\left(\frac{3}{64}f_1^2 + \frac{1}{16}f_1f_2 + \frac{1}{16}f_2^2\right)^2 + \left(f_0 + \frac{1}{4}f_1\right)^2 - 2n^2\left(\frac{3}{64}f_1^2 + \frac{1}{16}f_1f_2 + \frac{1}{16}f_2^2\right)\left(f_0 + \frac{1}{4}f_1\right)\right] + \left[\frac{A^2}{8} + \frac{B^2\mu^4}{8} + \frac{\mu^4C^2}{(1+\mu^2)^2} + \frac{\mu^4D^2}{(1+9\mu^2)^2} + \frac{\mu^4G^2}{(9+\mu^2)^2} + \frac{\mu^4H^2}{16(1+\mu^2)^2}\right] \tag{25}$$

Using Eqs. (9) and (16), the energy of bending W_2 of the shell can be calculated as

$$\frac{W_2}{\frac{1}{2}Etab} = \frac{1}{6(1-\nu^2)}\left(\frac{t}{R}\right)^2n^4\left[f_1^2\left\{\frac{1}{8}(1+\mu^2)^2 + \frac{1}{4}(1+\mu^4)\right\} + (1+\mu^4)f_1f_2 + (1+\mu^4)f_2^2\right] \tag{26}$$

The virtual work of the applied force can be obtained by means of Eqs. (10), (20), (23) and (24). The result is

$$\frac{W_3}{\frac{1}{2}Etab} = \left[2(1-\nu^2)\left(\frac{\sigma}{E}\right)^2 + n^2\frac{\sigma}{E}(\nu+\mu^2)\left\{\frac{3}{32}f_1^2 + \frac{1}{8}f_1f_2 + \frac{1}{8}f_2^2\right\} - 2\nu\frac{\sigma}{E}\left(f_0 + \frac{1}{4}f_1\right)\right] \tag{27}$$

Relation between the Compression Stress and the Amplitude of Waves

To find the relation between the average compression stress and the amplitude of the waves, the conditions which will make the expression $W_1 + W_2 - W_3$ a minimum have to be obtained. It was found that the calculations can be simplified to a certain extent by first using the condition that the sum of energies must be minimum with respect to f_0. Or

$$\frac{\partial}{\partial f_0}(W_1 + W_2 - W_3) = 0 \tag{28}$$

This condition determines a relation between f_0 and f_1, f_2, which can be written as:

$$f_0 + \frac{1}{4}f_1 = n^2\left(\frac{3}{64}f_1^2 + \frac{1}{16}f_1f_2 + \frac{1}{16}f_2^2\right) - \nu\frac{\sigma}{E} \tag{29}$$

Using this relation and Eq. (24), it is easily seen that $\alpha = 0$. In other words, the shell will expand radially to such an extent that the average of the circumferential stress σ_y is equal to zero. Substituting Eq. (29) into the expressions for W_1, W_2 and W_3 as given by Eqs. (25), (26) and (27) and using Eq. (18), the elastic energy of the system minus the virtual work is expressed finally in the following form:

$$\begin{aligned}\frac{W_1 + W_2 - W_3}{\frac{1}{2}Etab} = {} & -4\left(\frac{\sigma}{E}\right)^2 - \frac{\sigma}{E}n^2\mu^2\left(\frac{3}{8}f_1^2 + \frac{1}{2}f_1f_2 + \frac{1}{2}f_2^2\right) + n^4\left[\left\{\frac{1+\mu^4}{512} + \frac{17}{256}\frac{\mu^4}{(1+\mu^2)^2} + \frac{1}{64}\frac{\mu^4}{(1+9\mu^2)^2} + \frac{1}{64}\frac{\mu^4}{(9+\mu^2)^2}\right\}f_1^4 + \left\{\frac{9}{32}\frac{\mu^4}{(1+\mu^2)^2} + \frac{1}{16}\frac{\mu^4}{(1+9\mu^2)^2} + \frac{1}{16}\frac{\mu^4}{(9+\mu^2)^2}\right\}f_1^3f_2 + \left\{\frac{11}{32}\frac{\mu^4}{(1+\mu^2)^2} + \frac{1}{16}\frac{\mu^4}{(1+9\mu^2)^2} + \frac{1}{16}\frac{\mu^4}{(9+\mu^2)^2}\right\}f_1^2f_2^2 + \frac{1}{8}\frac{\mu^4}{(1+\mu^2)^2}f_1f_2^3 + \frac{1}{16}\frac{\mu^4}{(1+\mu^2)^2}f_2^4\right] - n^2\left[\left\{\frac{1}{64} + \frac{1}{4}\frac{\mu^4}{(1+\mu^2)^2}\right\}f_1^3 + \left\{\frac{1}{32} + \frac{1}{2}\frac{\mu^4}{(1+\mu^2)^2}\right\}f_1^2f_2\right] + \left[\left\{\frac{1}{32} + \frac{1}{4}\frac{\mu^4}{(1+\mu^2)^2}\right\}f_1^2 + \frac{1}{8}f_1f_2 + \frac{1}{8}f_2^2\right] + \frac{1}{6(1-\nu^2)}\left(\frac{t}{R}\right)^2n^4\left[\left\{\frac{1}{8}(1+\mu^2)^2 + \frac{1}{4}(1+\mu^4)\right\}f_1^2 + (1+\mu^4)f_1f_2 + (1+\mu^4)f_2^2\right]\end{aligned} \tag{30}$$

The equilibrium conditions are then obtained by differentiating this expression with respect to f_1 and f_2, and then set those derivatives equal to zero. The results can be written in a simpler form by introducing the following parameters:

$$\rho = \frac{f_2}{f_1}, \quad \eta = n^2\frac{t}{R}, \quad \xi = f_1\frac{R}{t} = \frac{\delta}{t} \tag{31}$$

where δ is the wave amplitude of the buckled shape of the cylindrical shell. Then the equilibrium conditions are

$$\begin{aligned}\frac{\sigma R}{Et}\eta\mu^2\left(\rho + \frac{3}{2}\right) = {} & (\eta\xi)^2\left[\frac{\mu^4}{4(1+\mu^2)^2}\rho^3 + \left\{\frac{11}{8}\frac{\mu^4}{(1+\mu^2)^2} + \frac{1}{4}\frac{\mu^4}{(1+9\mu^2)^2} + \frac{1}{4}\frac{\mu^4}{(9+\mu^2)^2}\right\}\rho^2 + \left\{\frac{27}{16}\frac{\mu^4}{(1+\mu^2)^2} + \frac{3}{8}\frac{\mu^4}{(1+9\mu^2)^2} + \frac{3}{8}\frac{\mu^4}{(9+\mu^2)^2}\right\}\rho + \left\{\frac{1+\mu^4}{64} + \frac{17}{32}\frac{\mu^4}{(1+\mu^2)^2} + \frac{1}{8}\frac{\mu^4}{(1+9\mu^2)^2} + \frac{1}{8}\frac{\mu^4}{(9+\mu^2)^2}\right\}\right] - (\eta\xi)\left[\left\{\frac{1}{8} + 2\frac{\mu^4}{(1+\mu^2)^2}\right\}\rho + \left\{\frac{3}{32} + \frac{3}{2}\frac{\mu^4}{(1+\mu^2)^2}\right\}\right] + \left[\frac{1}{4}\rho + \left\{\frac{1}{8} + \frac{\mu^4}{(1+\mu^2)^2}\right\}\right] + \frac{1}{3(1-\nu^2)}\eta^2\left[(1+\mu^4)\rho + \left\{\frac{1}{4}(1+\mu^2)^2 + \frac{1}{2}(1+\mu^4)\right\}\right]\end{aligned}$$

$$\begin{aligned}\frac{\sigma R}{Et}\eta\mu^2\left(\rho + \frac{1}{2}\right) = {} & (\eta\xi)^2\left[\frac{1}{4}\frac{\mu^4}{(1+\mu^2)^2}\rho^3 + \frac{3}{8}\frac{\mu^4}{(1+\mu^2)^2}\rho^2 + \left\{\frac{11}{16}\frac{\mu^4}{(1+\mu^2)^2} + \frac{1}{8}\frac{\mu^4}{(1+9\mu^2)^2} + \frac{1}{8}\frac{\mu^4}{(9+\mu^2)^2}\right\}\rho + \frac{9}{32}\frac{\mu^4}{(1+\mu^2)^2} + \frac{1}{16}\frac{\mu^4}{(1+9\mu^2)^2} + \frac{1}{16}\frac{\mu^4}{(9+\mu^2)^2}\right\}\right] - (\eta\xi)\left[\frac{1}{32} + \frac{1}{2}\frac{\mu^4}{(1+\mu^2)^2}\right] + \left[\frac{1}{4}\rho + \frac{1}{8}\right] + \frac{1}{3(1-\nu^2)}\eta^2\left[(1+\mu^4)\rho + \frac{1}{2}(1+\mu^4)\right]\end{aligned} \tag{32}$$

Eliminating $\sigma R/Et$ from the above equations, the following equation for ρ is obtained

$$A_3\rho^3 + A_2\rho^2 + A_1\rho + A_0 = 0 \tag{33}$$

where the coefficients are

$$\begin{aligned}A_3 = {} & (\eta\xi)^2\left\{\frac{3\mu^4}{(1+\mu^2)^2} + \frac{\mu^4}{(1+9\mu^2)^2} + \frac{\mu^4}{(9+\mu^2)^2}\right\} \\ A_2 = {} & (\eta\xi)^2\left\{\frac{9}{2}\frac{\mu^4}{(1+\mu^2)^2} + \frac{3}{2}\frac{\mu^4}{(1+9\mu^2)^2} + \frac{3}{2}\frac{\mu^4}{(9+\mu^2)^2}\right\} - (\eta\xi)\left\{\frac{1}{2} + \frac{8\mu^4}{(1+\mu^2)^2}\right\} \\ A_1 = {} & (\eta\xi)^2\left\{\frac{1+\mu^4}{16} + \frac{1}{4}\frac{\mu^4}{(1+\mu^2)^2} + \frac{1}{4}\frac{\mu^4}{(1+9\mu^2)^2} + \frac{1}{4}\frac{\mu^4}{(9+\mu^2)^2}\right\} - (\eta\xi)\left\{\frac{1}{2} + \frac{8\mu^4}{(1+\mu^2)^2}\right\} + \left\{\frac{4\mu^4}{(1+\mu^2)^2} - 1\right\} - \frac{2}{3(1-\nu^2)}\eta^2 \times \left\{2(1+\mu^4) - \frac{1}{2}(1+\mu^2)^2\right\}\end{aligned} \tag{34}$$

$$A_0 = (\eta\xi)^2\left\{\frac{1+\mu^4}{32} - \frac{5}{8}\frac{\mu^4}{(1+\mu^2)^2} - \frac{1}{8}\frac{\mu^4}{(1+9\mu^2)^2} - \frac{1}{8}\frac{\mu^4}{(9+\mu^2)^2}\right\} + \left\{\frac{2\mu^4}{(1+\mu^2)^2} - \frac{1}{2}\right\} - \frac{2}{3(1-\nu^2)}\eta^2\left\{(1+\mu^4) - \frac{1}{4}(1+\mu^2)^2\right\}$$

Therefore, when $\xi = 0$, *i.e.*, when the wave amplitude approaches zero Eq. (32) gives $A_2 = A_3 = 0$; and

$$A_1 = -\frac{2}{3(1-\nu^2)}\eta^2\left\{2(1+\mu^4) - \frac{1}{2}(1+\mu^2)^2\right\}$$

$$A_0 = -\frac{2}{3(1-\nu^2)}\eta^2\left\{(1+\mu^4) - \frac{1}{4}(1+\mu^2)^2\right\} = \frac{A_1}{2}$$

Substituting into Eq. (31) it is seen that $\rho = -1/2$, or $f_2 = -1/2 f_1$. Putting this relation between f_1 and f_2 into Eq. (14), the wave pattern is reduced to that represented by Eq. (13), *i.e.*, the wave pattern for infinitesimal wave amplitude given by the classical theory.

With a given value of μ and η, the coefficients for various values of the wave amplitude ξ can be first calculated by using Eq. (34). Then Eq. (33) can be solved for ρ corresponding to this particular set of values of μ and η at various wave amplitude ξ. When the value of ρ is known, Eq. (32) can be used to calculate the corresponding value of the "reduced compression stress," $\sigma R/Et$. It is found, however, that the following expression which is obtained from Eq. (30) by eliminating the third powers of ρ is more suitable for numerical computations:

$$\frac{\sigma R}{Et} = \left\{\frac{1}{\eta}\frac{\mu^2}{(1+\mu^2)^2} + \frac{1}{12(1-\nu^2)}\frac{\eta(1+\mu^2)^2}{\mu^2}\right\} + \frac{1}{\eta\mu^2}\left[(\eta\xi)^2\left\{\frac{\mu^4}{(1+\mu^2)^2} + \frac{\mu^4}{4(1+9\mu^2)^2} + \frac{\mu^4}{4(9+\mu^2)^2}\right\}\rho^2 + \left\{(\eta\xi)^2\left(\frac{\mu^4}{(1+\mu^2)^2} + \frac{1}{4}\frac{\mu^4}{(1+9\mu^2)^2} + \frac{1}{4}\frac{\mu^4}{(9+\mu^2)^2}\right) - (\eta\xi)\left(\frac{1}{8} + \frac{2\mu^4}{(1+\mu^2)^2}\right)\right\}\rho + \left\{(\eta\xi)^2\left(\frac{1+\mu^4}{64} + \frac{1}{4}\frac{\mu^4}{(1+\mu^2)^2} + \frac{1}{16}\frac{\mu^4}{(1+9\mu^2)^2} + \frac{1}{16}\frac{\mu^4}{(9+\mu^2)^2}\right) - (\eta\xi)\left(\frac{1}{16} + \frac{\mu^4}{(1+\mu^2)^2}\right)\right\}\right] \quad (35)$$

Therefore, when $\xi \to 0$, *i.e.*, when the wave amplitude becomes very small, Eq. (35) reduces to

$$\left(\frac{\sigma R}{Et}\right)_{\xi\to 0} = \frac{1}{\eta}\frac{\mu^2}{(1+\mu^2)^2} + \frac{1}{12(1-\nu^2)}\frac{1}{\frac{1}{\eta}\frac{\mu^2}{(1+\mu^2)^2}} \quad (36)$$

The minimum value of the average compression stress σ is given by

$$Min.\left(\frac{\sigma R}{Et}\right)_{\xi\to 0} = \frac{1}{\sqrt{3(1-\nu^2)}} \quad (37)$$

which is the well known result from the classical theory of infinitesimal deflections. This minimum value is obtained when

$$\frac{(1+\mu^2)^2}{\eta\mu^2} = 2\sqrt{3(1-\nu^2)} \quad (38)$$

It is interesting to notice that for infinitesimal wave amplitude, the minimum value of average compression stress occurs for an infinite number of pairs of the values of the parameters η and μ, for which the combined parameter shown in Eq. (38) has the same value.

Numerical computations were carried out for two values of the parameter μ, the ratio of the wave lengths in circumferential direction and in axial direction. These values of μ are 1 and 0.5. The value 1 was chosen because the experiments indicate that at large values of wave amplitude, the diamond waves have almost equal sides. The value 0.5 was chosen to investigate the possibility of occurrence of narrow waves. The results of these computations are shown in Fig. 2 and Fig. 3, where the reduced compression stress $\sigma R/Et$ is plotted against the wave amplitudes ξ. The parameter in the figures is η. The values written in the parenthesis after η are the actual number of waves n in circumferential direction for $R/t = 1000$. For given values of η and μ, *i.e.*, a fixed side of the wave, the load

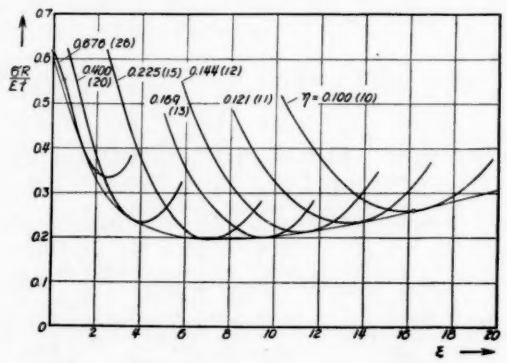

FIG. 2. Reduced compression stress $\sigma R/Et$ against amplitude of waves $\xi = \delta/t$, for $\mu = 1.00$ and different number of waves in circumferential direction.

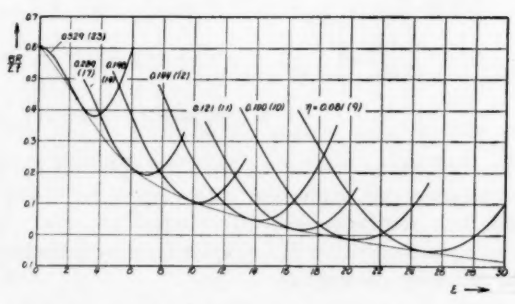

FIG. 3. Reduced compression stress $\sigma R/Et$ against amplitude of waves $\xi = \delta/t$, for $\mu = 0.50$ and different number of waves in circumferential direction.

sustained by the shell, $\sigma R/Et$ first decreases as the wave amplitude, ξ, is increased. After a minimum is reached, the load will rise with increase in wave amplitude. When the waves are larger, the initial buckling load, *i.e.*, the value of $\sigma R/Et$ at $\xi = 0$, is higher. However, the minimum load reached tends to a lower value, except for $\eta < 0.169$ and $\mu = 1$. For $\mu = 0.5$, the lowest value of the minimum load is not yet reached at $\eta = 0.081$.

The Relation between the Compression Stress and the Shortening of the Shell in the Axial Direction

Although the load characteristic of the cylindrical shell shown in the Figs. 2 and 3 gives the possible equilibrium relations between load and amplitude of the deflection wave, the actual behavior of a specimen in a testing machine cannot be directly seen from these figures. In a testing machine, the only factor under the control of the operator is the distance between the end plates; this is the geometrical restraint with which the specimen must conform. Therefore, in order to determine the behavior of the specimen the compression stress will have to be plotted as function of the end shortening. The unit end shortening, ϵ, *i.e.*, the total shortening in one wave length of the shell in axial direction divided by the wave length, can be easily calculated from Eq. (23). It is found that

$$\frac{\epsilon R}{t} = \frac{\sigma R}{Et} + \frac{\mu^2}{16}\xi(\eta\xi)(\rho^2 + \rho + \frac{3}{4}) \qquad (39)$$

This equation for the unit end shortening contains only quantities already found such as the values of ρ and $\sigma R/Et$. In Figs. 4 and 5, $\sigma R/Et$ is plotted against $\epsilon R/t$ for $\mu = 1$ and $\mu = 0.5$, respectively. It is immediately clear from these two figures that if the buckling process follows the curves drawn, after the shell starts to buckle the end shortening has to decrease. In other words, the end plates of the testing machine have to move apart. Therefore, the process of buckling in this region is highly unstable; as a matter of fact, before the operator has time to separate the end plates, the shell will jump to the point P (Figs. 4 or 5) which corresponds to the same end shortening as the starting point of the buckling process, but to a much lower compression stress. This jump in equilibrium position involves a release of elastic energy and thus explains the rapidity of the buckling process and the accompaning vibration.

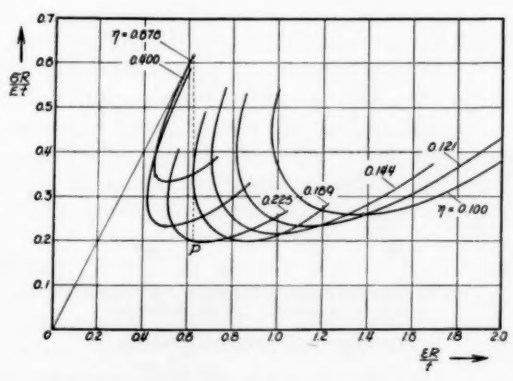

FIG. 4. Reduced compression stress $\sigma R/Et$ against unit end shortening $\epsilon R/t$, for $\mu = 1.00$ and different number of waves in circumferential direction.

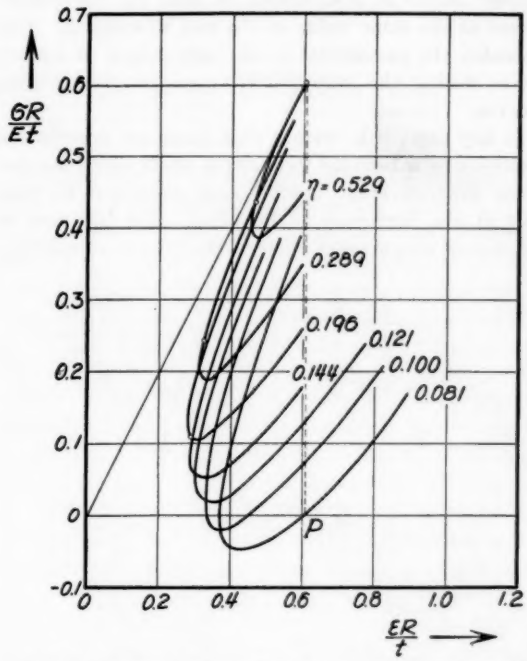

FIG. 5. Reduced compression stress $\sigma R/Et$ against unit end shortening $\epsilon R/t$, for $\mu = 0.50$ and different number of waves in circumferential direction.

It is tacitly assumed in the previous paragraph that if the system has an equilibrium position corresponding to the same end conditions, *i.e.*, same end shortening, but involving a lower value of σ or a lower value of the stored elastic energy, a transition to one of these equilibrium positions will actually take place. This is not based on any vigorous application of the principles of mechanics. It is evident that if, for example, the straight equilibrium position is stable, *i.e.*, all infinitesimally near configurations have higher energy, such a transition can only take place by application of an external impulse of finite magnitude. However, it can be assumed that such impulses will always be present in an experiment performed without extraordinary precaution in this respect, and of course if the structure is used in service. Then again, if it is assumed that the structure is helped over the "energy hump" by such external impulse, it cannot be proved that the jump has to end in the equilibrium position with the lowest energy level. However, if it is exposed

to several random impulses, there is a certain probability that the position with the lowest energy level will be the "journey's end." An approximate calculation of the elastic energy of the shells shows that for large values of $\epsilon R/t$ and $\eta < 0.121$, the elastic energy of the narrow waves is higher than that of the square waves at same value of the end shortening. Therefore, under such conditions the narrow waves appear to be less probable. However, for $\epsilon R/t$ near 0.6, and $\eta \geqq 0.121$ the elastic energy stored in the shell for the narrow waves is comparable to that for the square waves at the same value of the end shortening. This indicates the possibility of the appearance of narrow waves during the very initial stages of the buckling process.

In any case, it is certain that there are equilibrium positions of a buckled cylindrical shell which involve much lower average compression stress $\sigma R/Et$ than that at the beginning of buckling. For instance, in the case of square wave pattern, the lowest compression stress is given by

$$\frac{\sigma}{E} = 0.194\frac{t}{R} \tag{40}$$

Incidentally, this value corresponds closely to most of the experimental results obtained by L. H. Donnell[3] and E. E. Lundquist.[7]

The corresponding value of the parameter η which determines the number of waves is equal to 0.225. In case of $R/t = 1000$, the number of waves, n, will be 15 which also agrees well with the experimental evidence. For this particular value of the radius to thickness ratio, the number of waves along the circumference decreases from the $n = 26$ at the beginning of the buckling to $n = 15$ at the calculated minimum buckling stress. This gradual increase in the size of waves with the unit shortening is also observed by the experiments reported in an earlier paper.[2]

It is particularly interesting, however, to trace the gradual change in the wave pattern during the buckling process. Figs. 6 and 7 show the lines of equal deflection of the wave surfaces corresponding to different equilibrium states for two values of the aspect ratio of the wave pattern, $\mu = 1.0$ and $\mu = 0.5$. These particular equilibrium states are denoted in Figs. 2, 3, 4 and 5 by small circles in order to indicate their rela-

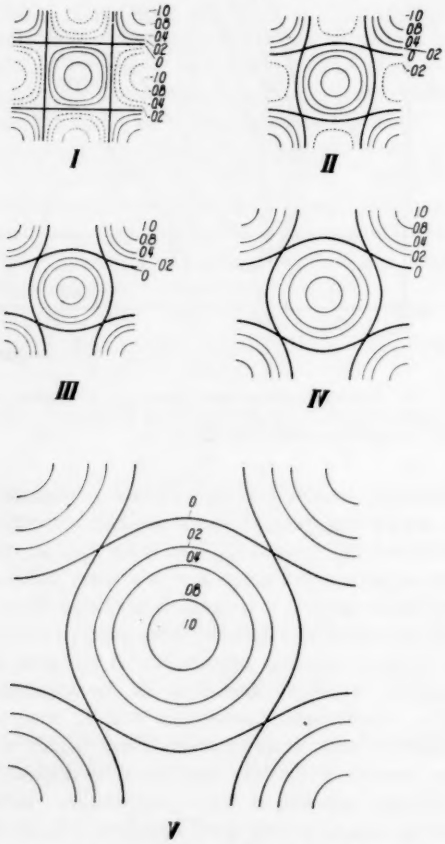

FIG. 6. Lines of equal deflection of wave surfaces. +1.0 = maximum inward deflection.

Compression in vertical direction

$\mu = 1.00$

	ξ	η
I	0	0.676
II	1.00	0.676
III	2.00	-0.676
IV	4.00	0.400
V	16.22	0.100

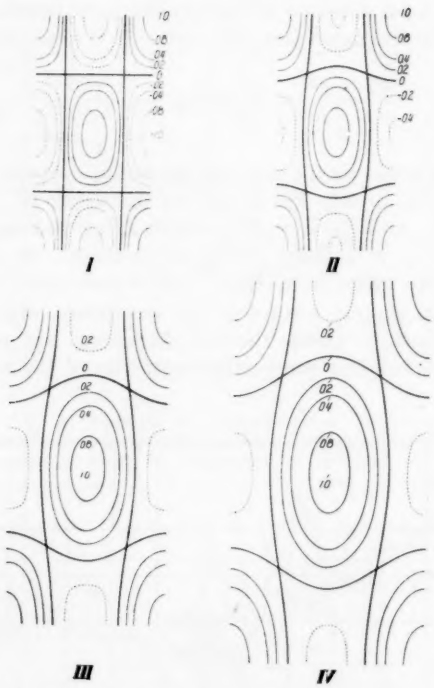

Fig. 7. Lines of equal deflection of wave surfaces. +1.0 = maximum inward deflection.

Compression in vertical direction

$\mu = 0.500$

	ξ	η
I	0.00	0.529
II	2.50	0.529
III	5.50	0.289
IV	10.00	0.196

tive position during the buckling process. It is seen that there is a rapid shift from the rectangular waves bounded by lines, x = const., and y = const., as predicted by the classical theory for infinitesimal wave amplitudes, to staggered rows of circular or elliptical waves. Whereas, the rectangular waves are directed alternatively inward and outward, the circular or elliptical waves are all directed inward. The transition is practically completed for $\xi = 4$ or 6, *i.e.*, when the wave amplitude is only 4 or 6 times the thickness of the shell. The occurrence of such inwardly directed circular and elliptical waves at this stage of the buckling process is in good agreement with the experimental observations.[2] If the experiment is continued to larger deflections ($\xi \sim 60$), these staggered waves acquire the characteristic diamond shape. The present approximate theory fails to give these sharp diamond shaped waves. It is obviously not sufficiently exact for such large deflections. Furthermore, when these diamond shaped waves occur, the load on the specimen actually falls to a very low value such as $\sigma R/Et \simeq 0.06$, whereas the theory shows a slight increase of the stress at least for the case $\mu = 1.0$. Therefore, the present calculation can be only considered as a fair approximation to the earlier stages of buckling when the wave amplitude is only a few times the thickness of the shell. Nevertheless, it reproduces the characteristic features of the buckling process observed in the laboratory.

The Effect of the Elastic Characteristic of the Testing Machine on the Buckling Phenomenon

It was stated in the previous paragraph that the state of the specimen is determined by the distance between the end plate and that this distance is the independent parameter controlled by the experimenter. This statement is correct only insofar the elasticity in the mechanism of the testing machine is neglected. There is always a certain amount of elastic deflection in the loading mechanism and this deflection is a function of the load. Hence, if, for example, the loading crank is held at a certain position, the compression force acting on the specimen will force the end plates apart and thus reduce the amount of end shortening of the specimen. The actual shortening is determined by the load-deflection characteristics of the specimen and the testing machine. Assuming that the testing machine has a linear elastic characteristic, the compression load is related to the end shortening by parallel straight lines, each line corresponding to, say, a fixed number of turns of the loading crank. If the loading crank of the machine is held at a fixed position, corresponding values of the compression load and end shortening of the specimen must lie on the straight line for this crank position. If the load-end shortening characteristics of the specimen itself are given, it is evident that the equilibrium positions of the entire system are determined by intersections of the curves representing the characteristics of the specimen with the straight lines representing the characteristics of the machine.

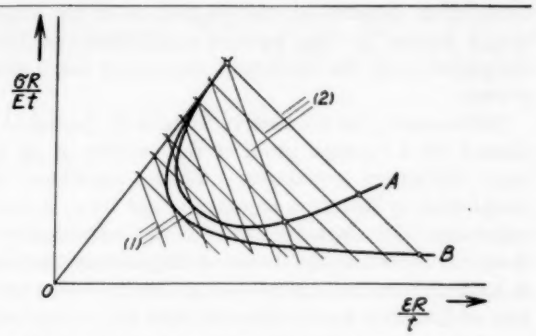

FIG. 8. Effect of rigidity of testing machine on behavior of specimen.
(1) Represents a more rigid machine.
(2) Represents a less rigid machine.

Fig. 8 shows representative curves for the characteristics of the specimen and two families of straight lines representing the characteristics of two different testing machines. It is evident that after the maximum or initial buckling load is reached, the shell will jump to a new equilibrium position involving much lower compression load. But this new equilibrium position is determined not only by the load-end shortening relationship and also by the elastic characteristic of the testing machine. A more elastic machine will give a set of characteristic straight lines with smaller slopes. Therefore, in case of curve A (Fig. 8), a more elastic machine will make the shell to jump to a higher load, while in case of curve B, a more elastic machine will make the shell to jump to a lower load. This influence of the elasticity of the testing machine has been discussed by the senior author in connection with the plastic buckling of columns.[8]

Conclusions

In the previous paragraphs, the authors have shown that there are equilibrium positions with buckled shape involving much lower load than the buckling load predicted by the classical theory, and thus if the specimen is slightly imperfect, it is reasonable to expect much lower buckling loads. They have also pointed out that the elastic characteristic of the testing machine might have quite a large influence on the buckling process and this might be another cause of the large scattering of the data obtained by different experimenters. However, due to the complexity of the problem, the results given in this paper can be only considered as a rough approximation and most of the statements made are qualitative rather than quantitative. To put the new theory on a solid footing, a more accurate solution of the differential equations of equilibrium is necessary. Particular attention must be given to the calculation of the elastic energy stored in the shell, because it is found that the most probable

equilibrium depends on the magnitude of the elastic energy stored in the various equilibrium positions compatible with the constraint exerted by the loading process.

Furthermore, an inquisitive mind will, perhaps, be pleased by a rigorous proof of the validity of all the large deflection equations. These equations are established by intuitive arguments, not by systematic reasoning. For instance, due to the appearance of sharp curvatures in the diamond shaped wave surfaces at large deflections, it is not certain whether the curvature of the shell has to be calculated more accurately by taking into account the second order terms, or the extensions of the median surface should be more accurately determined. It is the belief of the authors that an investigation of these problems by starting from the general non-linear theory of elasticity developed by G. Kirchhoff, J. Boussinesq and others is very desirable. The recent work by R. Kappus[9] is a noteworthy contribution in this field of investigation. The senior author has already expressed this opinion in his 1939 Gibbs Lecture[10] given before the American Mathematical Society.

References

[1] von Kármán, Th., and Tsien, Hsue-Shen, *The Buckling of Spherical Shells by External Pressure*, Journal of the Aeronautical Sciences, Vol. 7, No. 2, page 43, December, 1939.

[2] von Kármán, Th., Dunn, Louis, G., and Tsien, Hsue-Shen, *The Influence of Curvature on the Buckling Characteristics of Structures*, Journal of the Aeronautical Sciences, Vol. 7, No. 7, page 276, May, 1940.

[3] Donnell, L. H., *A New Theory for the Buckling of Thin Cylinders Under Axial Compression and Bending*, A.S.M.E. Transactions, Vol. 56, pages 795–806, November, 1934.

[4] Flügge, W., *Die Stabilität der Kreiszylinderschale*, Ingenieur-Archiv, Vol. 3, pages 463–506, 1932.

[5] von Kármán, Th., Encyklopädie der Mathematischen Wissenschaften, IV.4, page 349, 1910.

[6] Donnell, L. H., *Stability of Thin-Walled Tubes Under Torsion*, N.A.C.A. Technical Report No. 479, 1934.

[7] Lundquist, E. E., *Strength Tests of Thin-Walled Duralumin Cylinders in Compression*, N.A.C.A. Technical Report No. 473, 1933.

[8] von Kármán, Th., *Untersuchungen über Knickfestigkeit*, Forchungsarbeiten, No. 81, Berlin, 1910.

[9] Kappus, R., *Zur Elastizitätstheorie endlicher Verschiebungen*, ZAMM, Vol. 19, pages 271–285, 344–361, 1939.

[10] von Kármán, Th., *The Engineer Grapples with Nonlinear Problems*, Bulletin of the American Mathematical Society, Vol. 46, pages 636–637, 1940.

Letter to the Editor

April 25, 1941

Dear Sir:

In reply to Dr. Nagel's *Letter to the Editor*, published in the April, 1941, issue of the Journal, the authors[1] of the article in question would like to point out that no discrepancies exist between their results and those of Theodorsen.[2] On the contrary, since their charts are based upon the fundamental Theodorsen equations, complete agreement exists.

Dr. Nagel has stated that the two finite flutter speeds, shown for the example on page 501[1] are in contradiction to the graphs of Theodorsen on page 18.[2] Dr. Nagel will find on closer examination that the example given in the paper,[1] using an aileron radius of gyration parameter $r_\beta^2 = 0.001$ is not covered in Theodorsen's Graph II-B where the minimum value used is $r_\beta^2 = {}^1/_{120}$ for a corresponding value of $c = 0.5$. Moreover, if the r_β^2 value on page 501[1] is increased to ${}^1/_{120}$, the results obtained from the chart will be in exact agreement with Theodorsen's Graph II-B. This point has been discussed with and verified by Dr. Theodorsen.

While Dr. Nagel believes that values of the aileron-wing bending frequency ratio $(\omega_\beta/\omega_h) < 1$ are most commonly encountered, the studies of Lombard,[3] compiled from extensive test data, indicate that the opposite is true. However, it is apparent from the mathematical development of the paper that the chart computations may be extended to include frequency ratios below unity. When this is done, and Fig. 19[1] on page 507 extended, it will be found that the curves exhibit a sharp change in slope at $\omega_\beta/\omega_h = 1$ and cross the $\omega_\beta/\omega_h = 0$ axis at a finite value of x_β instead of approaching an asymptote at $\omega_\beta/\omega_h = 1$ as Dr. Nagel has inferred.

The authors[1] agree with Dr. Nagel that charts for the three-degrees-of-freedom case would be desirable. The present two degree charts, however, have eliminated extensive computation and also furnish an excellent means of illustrating flutter criteria to the designer not familiar with the analytical details.

William B. Bergen and Lee Arnold
The Glenn L. Martin Company

[1] Bergen, W. B., and Arnold, Lee, *Graphical Solution of the Bending-Aileron Case of Flutter*, Journal of the Aeronautical Sciences, Vol. 7, No. 12, October, 1940.

[2] Theodorsen, Th., and Garrick, I. E., *Mechanism of Flutter*, N.A.C.A. Technical Report No. 685, 1940.

[3] Lombard, A. E., Jr., California Institute of Technology Thesis, Publication No. 116, Figs. 57 and 59, 1939.

Some Experimental Results on Wing Flutter

WILLIAM BOLLAY AND CHARLES D. BROWN
Harvard University

SUMMARY

The present paper represents a progress report of some experiments being carried out in the aerodynamics laboratory of Harvard University. The first part of the experimental investigation consisted in the measurement of the vibration response curves of a wing in the wind tunnel. A wing, free to vibrate in bending and in torsion, was subjected to a forced vibration at various air speeds up to the flutter speed. These measurements are of interest in that they show how the two natural frequencies of the wing come together as the flutter velocity is approached. The peaks of these response curves are also of interest in that they determine the maximum stresses which are experienced, for instance, by a propeller which is subjected to periodic impulses from the engine.

The second part of the investigation deals with the problem of flutter above the stall. Measurements show that at angles of attack above the positive stalling angle and below the negative stalling angle the flutter speed is decreased to less than one-third of the flutter speed of the unstalled wing. This flutter seems to be associated with an instability which arises when the slope of the lift curve becomes negative. Experiments on a metal wing supported as a cantilever indicate that the flutter at the stall may also be associated with an excitation from a system of Kármán vortices.

VIBRATION RESPONSE OF A WING IN THE WIND TUNNEL

THE EXPERIMENTAL setup for the determination of the vibration response characteristics of a wing was as follows: The wing was supported in the working section of the Harvard One-Meter Wind Tunnel as shown in Fig. 1. The wing was mounted horizontally

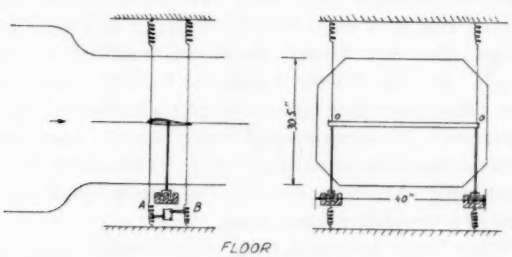

FIG. 1.

on a set of springs which permitted the wing to rotate as well as to deflect up and down, thus simulating the torsion and bending of an airplane wing. A set of long fore-and-aft and side wires restrain the wing from motion in these directions. A sinusoidal up-and-down force, $P = P_0 \sin \omega t$ is applied by an electrodynamic exciter at each wing tip. The two wing tips are excited in phase so that the lateral axis OO' has a uniform up-and-down motion. The axis of force application does not in general coincide with the axis of the center of gravity and thus the vertical motion of the driving rods sets up also a rotational motion of the wing about the lateral axis OO'.

The tests were carried out in the following manner. At a fixed value of the air velocity the frequency of excitation was varied from about 3 to 30 cycles per second and the corresponding amplitudes of motion of the wing were observed. This gives response curves of the type shown in Fig. 2 for various air velocities.

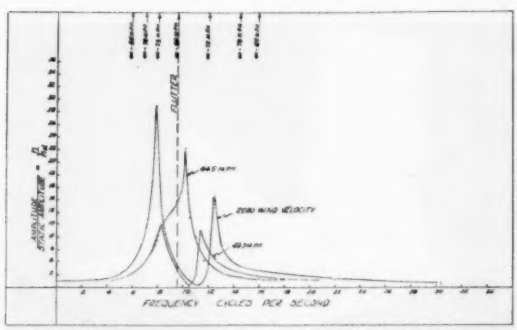

FIG. 2. Experimental curves giving bending amplitude of the axis of twist against frequency of excitation for various wind velocities.

The intensity of excitation P_0 was kept constant throughout the test. Two wings were studied in this manner. In the test of wing I the amplitudes of motion of the two spring wires A and B were recorded on a rotating drum. From this record the amplitudes, phase angles and frequencies of the motions can be determined.

Fig. 2 represents the result of such a set of calculations, namely the vertical amplitude of motion of the elastic center of wing I. It will be observed that the response curve at a fixed air speed has two resonance peaks corresponding to the two natural frequencies of the two-degrees-of-freedom system. As the air velocity is increased from zero, the maximum amplitude of these peaks is reduced by the positive air damping (Fig. 3a), and the two natural frequencies approach each other (Fig. 3b). If the air speed is increased sufficiently, the two natural frequencies come together, and the resonance amplitude becomes infinite. The corresponding air speed and frequency are called the "flutter speed" and "flutter frequency," respectively, and the point on the V–ω plane at which this coincidence occurs is called the "flutter point."

Presented at the Aerodynamics session, Ninth Annual Meeting, I.Ae.S., New York, January 31, 1941.

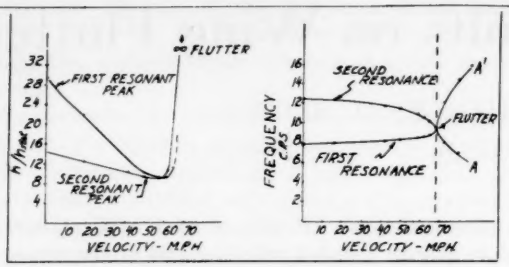

FIG. 3a. Maximum amplitude of resonance peaks as function of wind velocity.

FIG. 3b. Resonant frequencies as functions of wind velocities.

A photograph of the surface representing the amplitude response of the system as a function of velocity and frequency of excitation is shown in Fig. 4. It will be observed that this surface extends even into the region of velocities above the flutter velocity. This is shown

FIG. 4. Photograph of surface showing the amplitude response as a function of velocity v and frequency ω.

best by the curve AA' in Fig. 3b which represents the boundary between a finite and an infinite response of the system. Apparently the velocity at which an infinite response is obtained is higher than the flutter velocity if excitation occurs at a frequency different from the flutter frequency. This fact is actually of little practical importance because if there are any disturbances present in the air stream or if a shock is applied to the system which contains even a small Fourier component having the flutter frequency, then this component is magnified tremendously and flutter is started. Fig. 5 shows the phase angle between the amplitude at the elastic center and the angle of twist α. Both Figs. 4 and 5 indicate that the motion corresponding to wing flutter is more nearly of the type corresponding to the second natural frequency, that is, principally an angular motion with node close to the center of gravity.

A theoretical calculation of the amplitude response of wing I as a function of velocity and frequency of excitation was carried out according to the method suggested by Theodorsen and Garrick. The theoretical resonance frequencies checked very closely with those of Fig. 3b. The theoretical maximum amplitude response curves were similar to those in Fig. 3a except that at zero airspeed they approached infinity. This was due to the fact that the theoretical calculation was carried out on the assumption that there was no material damping.

The characteristics of wing I were as follows:

Material	Balsa wood
Span	30 inches
Chord	10 inches
Airfoil section	N.A.C.A. 0015
Angle of attack	0°
Wing mass/mass of air	76
"Uncoupled" bending frequency $\omega_\alpha = \sqrt{\frac{C_\alpha}{I_\alpha}}$	= 64.1 rad./sec.
"Uncoupled" torsional frequency $\omega_h = \sqrt{\frac{C_h}{M}}$	= 55.9 rad./sec.
Position of elastic axis	.425 chords back of leading edge
Position of center of gravity	.55 chords back of leading edge
Position of point of force application	.425 chords back of leading edge
Experimental flutter speed 68 m.p.h.	Finite wing
Experimental flutter frequency 9.60 cycles/sec	Finite wing
Theoretical flutter speed 62 m.p.h.	Two-dimensional wing
Theoretical flutter frequency 9.54 cycles/sec	Two-dimensional wing

The results shown in Figs. 2 to 5 were obtained with the above wing extended across the 40 inch working section of the tunnel. In order to find the effect of the finite span a set of end-plates was attached to the wing and two-dimensional flow conditions were further approached by inserting a longitudinal plate into the tunnel on each side of the wing. The resulting resonance curves were very similar to those shown in Figs. 2 to 5 except that the flutter speed was reduced to 60.8 m.p.h. and the flutter frequency to 8.92 cycles/sec. The theory therefore appears to give satisfactory agreement with the experimental flutter speeds when two-dimensional flow conditions exist. The effect of the finite wing span is to increase the flutter speed above that of a two-dimensional wing.

Wing I was destroyed by a violent flutter, and thus

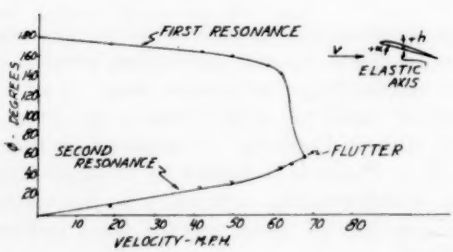

FIG. 5. Phase angle between the bending and the torsional motion.

for the further investigations wing II, which happened to be available, was used. The characteristics of wing II are as follows:

Material	Mahogany wood
Span	$39^1/_2$ inches
Chord	$6^3/_4$ inches
Airfoil section	N.A.C.A. 23012
Angle of attack	Variable
Wing mass/apparent mass of air	161.2
"Uncoupled" bending frequency $\omega_h = \sqrt{\frac{C_h}{M}}$	= 80.3 rad./sec.
"Uncoupled" torsional frequency $\omega_\alpha = \sqrt{\frac{C_\alpha}{I_\alpha}}$	= 87.2 rad./sec.
Position of elastic axis	.355 chords back of leading edge
Position of center of gravity	.469 chords back of leading edge
Position of point of force application	.25 chords back of leading edge

Wing II was equipped with 10 inch end-plates, which were within one-fourth inch of the tunnel walls, and thus the flow was practically two-dimensional. In the test of this wing the response curves were obtained by measuring the linear displacement of the driving rods and the angular displacement of the wing with respect to the driving rods.

The pick-up element in each case consisted of a small resistor which had a 45 volt battery connected across it (Fig. 6). A stationary contactor picks off the intermediate voltage. Two vacuum-tube voltmeters were

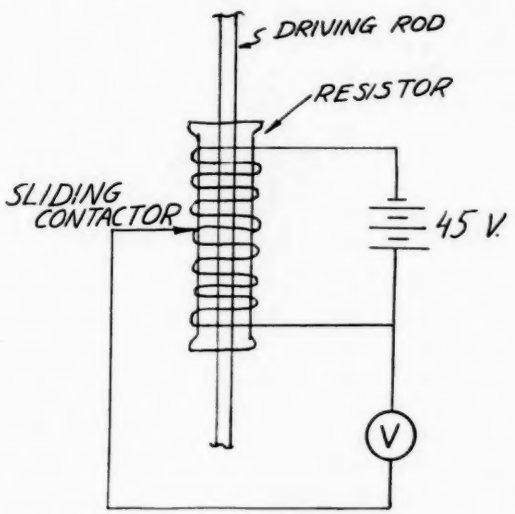

FIG. 6. Pick-up element for measuring motion.

used to determine the linear and angular displacement of the wing at the driving point. The phase angles between the two motions can be determined approximately by measuring Lissajou figures on a cathode ray oscillograph; however, this did not prove to be a very accurate method and therefore was used only for qualitative observations of the phase shifts.

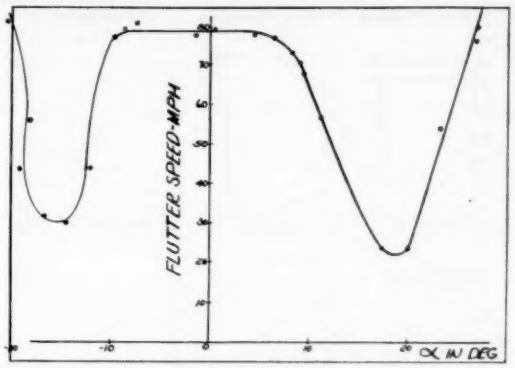

FIG. 7. Flutter speed of wing II as a function of angle of attack α.

A set of linear and angular response curves were obtained for a forced vibration $P = P_0 \sin \omega t$ applied through the driving rods to the axis OO' (Fig. 1). These response curves are similar to those obtained on wing I.

The variation of flutter speed with angle of attack was also investigated with wing II. To vary the angle of attack the wing was turned; the spring system was kept normal to the free stream velocity, that is, in the lift direction. Fig. 7 shows the result of this test. The flutter speed is constant, within the limits of experimental error, as long as the wing is not stalled. As the positive or negative stalling angles are approached the flutter speed decreases very markedly* reaching a minimum at the point at which the lift curve has a sharp drop (Fig. 8). For larger absolute values of the angle of attack the flutter speed increases again. It will be observed that the region of minimum flutter speed coincides with the maximum negative slope of the lift curve (Fig. 8) and probably corresponds to a periodical

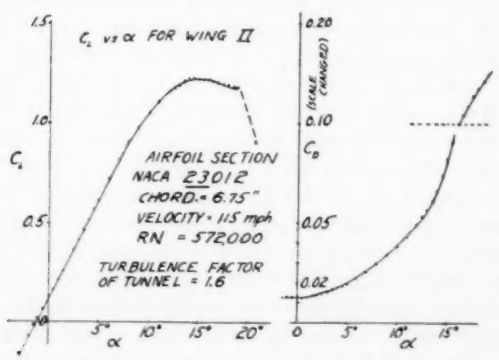

FIG. 8. Aerodynamic characteristics of wing II.

change of the point of flow separation. The decrease in flutter speed starts already at an angle of attack of about 7°, which is where the lift curve starts to break

* Similar decreases in flutter speed have been observed by Studer, H. L., *Mitt. aus d. Inst. f. Aerodyn. E.T.H.*, Zürich, 1936.

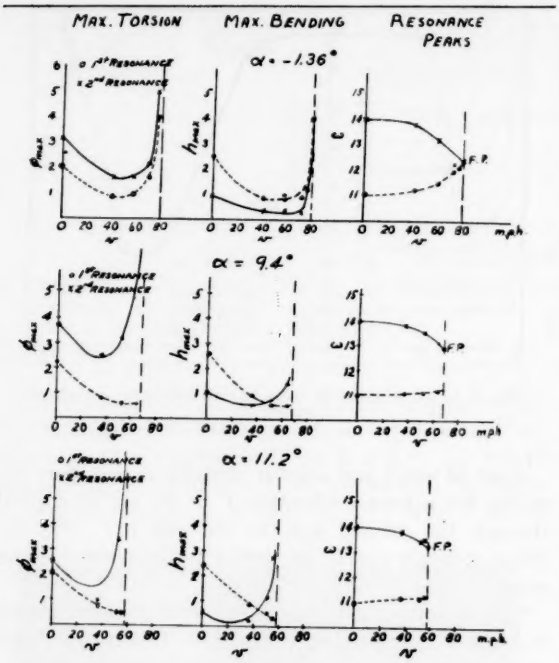

FIG. 9. Maximum amplitude response in bending and torsion as functions of air velocity.
Scale: Torsion 1 unit = .418 degrees
Bending 1 unit = 1.18 mm.

away from a straight line. Figs. 9a to c represent peaks of the response curves of wing II at various angles of attack. The up-and-down motion of the wing will in brief be called the "bending," the angular motion the "torsion" of the wing. It is seen that in each case there is first a decrease in maximum amplitude as the air speed is increased, corresponding to positive air damping and then a sharp increase in amplitude as the flutter speed is approached. The position of the resonance peaks on the ω–v plane shows that below the stall at $\alpha = -1.36°$ the flutter point corresponds to the intersection of the two resonance peaks. In the stalled region at $\alpha = 9.4°$ and $11.2°$ the flutter point lies on the second resonance peak and correspondingly the flutter frequency rises from 12.3 cycles per second to 13 cycles per second at $\alpha = 9.40°$, 13.2 cycles at $\alpha = 11.2°$ and 13.7 cycles at $\alpha = -16.6°$. A particularly steady type of flutter was observed at an angle of attack of 11.2°. Judging by streamer observations the rear 40% of the upper surface seemed to be stalled, and as seen on the C_L *vs.* α curve this point lies on the curved portion of the lift curve before the peak. The wing vibrated without external excitation at a relatively small bending amplitude and a torsional amplitude of $\pm 2.1°$ at an air speed of 57 m.p.h.

The above results indicate quite clearly that the self-induced vibrations which exist at the stall are of a different nature from those below the stall. There is a continuous transition from the first type of critical vibration to the second and since they are both self-induced vibrations the name "flutter" has been applied to both. The minimum flutter speed at the stall occurs at the angles of attack at which the slope of the lift curve is most strongly negative. This fact has been observed in connection with other phenomena, for instance the "galloping" of transmission lines, and has been explained by J. P. Den Hartog* as follows: If $dC_L/d\alpha$ is negative then the lift force is increased as the wing moves upward and decreased as it moves downward during a vibration, and thus the vibration continues to build up. The interpretation of this flutter at the stall in terms of the static lift curve of the wing is of course an approximation. It has been shown by W. S. Farren† that the dynamic lift curve is different in the vicinity of the stall. The maximum lift coefficient is higher when the angle of attack is suddenly increased and the wing may well run through a hysteresis loop near the stall, as suggested by Studer, and thus obtain additional energy out of the air stream. This type of behavior is suggested by the experimental results at $\alpha = 9.4°$ and $\alpha = 11.2°$, which are both at angles below that corresponding to the peak of the static lift curve.

The above explanation still leaves unsolved the question of what determines the flutter velocity and flutter frequency at the stall. It would be expected and this fact is borne out by the experiments on wing II that the frequency of the flutter is at one of the natural frequencies of the wing which vary, of course, with the air speed. Since the torsional motion was the easier one to excite it was not surprising that the flutter took on the second natural frequency which corresponded more nearly to a purely torsional motion. The question of what determines the flutter speed is a much more difficult one to answer. Probably this question has to be answered on the basis of energy considerations. The aerodynamic driving force in torsion is proportional to the square of the wind velocity and the amplitude of motion. The damping forces in the wing are proportional to the amplitude of motion independent of the air velocity. Whenever the work done by the aerodynamic driving force during a cycle exceeds the work done against the damping forces, the resonance amplitude will become infinite. The only method of estimating the flutter speeds at the stall would be on the basis of assumed values of $dC_L/d\alpha$ or of an assumed hysteresis curve up near the stall. Measurements of these variables and a correlation with the damping factors of the wing should prove to be of interest.

FREE VIBRATIONS OF A CANTILEVER WING AT THE STALL

A solid dural cantilever wing of $38\frac{1}{2}$ inch span, $6\frac{3}{4}$ inch chord and 0.5 inch thickness was kindly supplied by the Hamilton Standard Propeller Company together with a heavy base for mounting the wing in the wind tunnel. The airfoil section was a modified Clark

* Den Hartog, J. P., *Mechanical Vibrations*, page 343, 1940.
† Farren, W. S., Reports and Memorandum No. 1648, 1935.

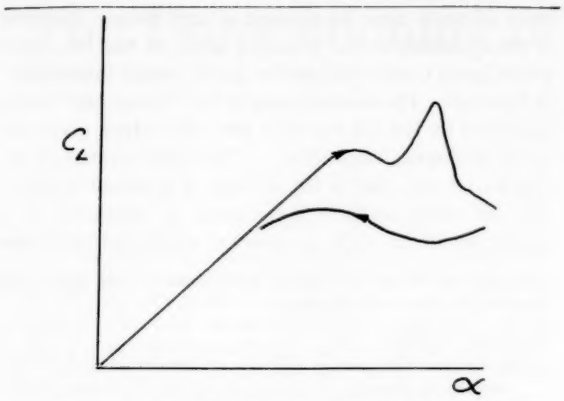

FIG. 10. "Hysteresis Loop" near the stall (according to Farren).

Y with a flat lower surface. The wing, henceforth denoted as wing III, was mounted vertically in the working section of the tunnel, the lower edge of the cantilever flush with the tunnel floor and the free edge extending out through the upper wall of the tunnel. The calculated flutter speed of this wing was so high (900 m.p.h.) that measurements of response curves to forced vibrations below the stall did not appear to be very useful. At the stall it was found, however, that this wing built up steady vibrations the intensity of which seemed to vary with wind velocity. In order to measure the magnitude of the vibration a carbon stress gage of the type developed by Mr. C. Kearns of the Hamilton Standard Propeller Company was glued to the root of the cantilever wing, and at an angle of attack of $14^1/_2°$ the stress record shown in Fig. 11 was obtained. At a very low wind speed a faint oscillation of the wing in its first bending mode occurred. At a velocity of about 47 m.p.h. a pronounced second mode bending vibration of the wing occurred with a tip amplitude of about ± 1.1 mm. (corresponding to a stress at the root of about 1800 lbs./in.^{2}). This second mode vibration died out again as the air speed was increased and gave way to a third mode bending vibration which reached its peak at about 128 m.p.h. The frequency of motion of the wing in each case corresponded to the natural frequency in bending in the first, second or third mode, as indicated by the small circles in Fig. 10. This phenomenon looked very much like an excitation by Kármán vortices,* and thus a hot-wire anemometer was used to check this assumption. The frequency of the vortices was measured both with the wing tip clamped at the top so that it could not vibrate as well as with the wing tip free. The results are shown in Fig. 10. The vortex frequency with wing tip fixed is given by the dimensionless Kármán constant

$$K = \frac{\omega c \sin \alpha}{v}$$

* Durand, W. F., *Aerodynamic Theory*, Vol. 2, page 342, Julius Springer, Berlin, 1934.

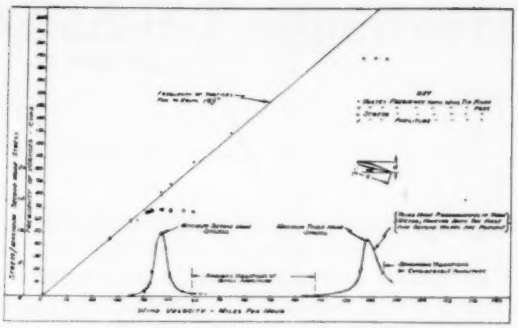

FIG. 11. Curves showing vortex frequencies, alternating stress frequencies and maximum stress as functions of wind velocities.

where $\alpha = 14^1/_2°$, $K = .167$ if ω is the vortex frequency in cycles per second, c is the blade chord in feet, α is the angle of attack and v is the air velocity in feet per second. The width of the wake d has been approximated in the above definition by the projected height of the airfoil. When the airfoil is free to vibrate the width d is greater than $c \sin \alpha$ and thus the constant K is less. As a result the eddy frequency is decreased when large vibrations occur.

These results show that the Kármán vortices give an excitation with a frequency directly proportional to the air velocity. At certain discrete air velocities the Kármán vortex frequency will coincide with one of the natural frequencies of motion of the wing. Whenever this occurs, vibrations of the wing build up. The hot-wire results given in Fig. 11 for the second bending frequency indicate that the vortex frequencies fall in step with the natural frequency of the wing for a small range of velocities and then revert to the straight line curve again.

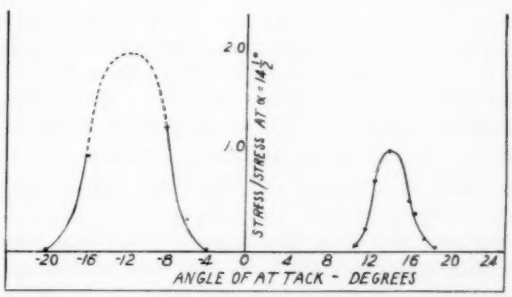

FIG. 12. Maximum response of cantilever wing III in the second bending mode (no external excitation).

The magnitude of the maximum vibration of the wing in the second mode as a function of angle of attack is shown in Fig. 12; the curve of C_L *vs.* α for wing III is given in Fig. 13. These graphs indicate that at least for wing III the "flutter at the stall" is a vibration excited by a Kármán vortex system.

The intensity of this vibration of wing III was not

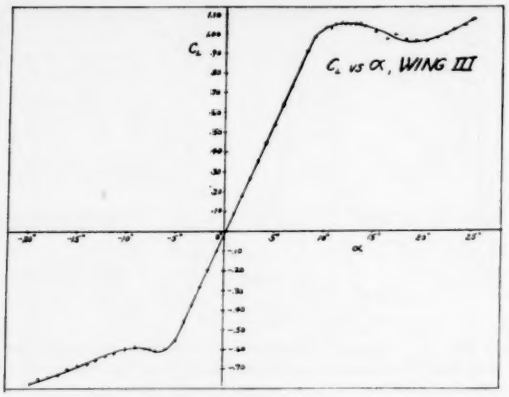

FIG. 13. Aerodynamic characteristics of wing III.

sufficiently severe to cause a dangerous dynamic instability of the wing. The excitation may, however, be of importance from the standpoint of fatigue stresses on structures such as propellers.

The study of the vibration characteristics of wing III at the stall is being continued as there are indications that at $\alpha = -20°$ at a speed of 127.5 m.p.h. a very violent vibration builds up, principally in the first mode of bending. This violent vibration is probably due to the "hysteresis" curve at the stall rather than the Kármán vortex excitation. Similarly the flutter for wing II at $\alpha = 17.4°$ does not seem to be related to the Kármán vortex excitation. The value of K in the latter case was .066 while Kármán vortex excitation seems to occur in the range $K = .16$ to .22.

CONCLUSIONS

There appear to be at least three possible sources of excitation of wing vibrations at the stall and two or more of these may be present at any time. The first of these causes is the negative slope of the lift curve which leads to what might be called "static instability" at the stall. The second cause is the "hysteresis" curve described by the lift curve at the stall, which gives rise to a "dynamic instability." The third source of excitation at the stall is the system of Kármán vortices. The net effect of these three types of excitation is to lower considerably the air speed at which flutter occurs.

Among the recent references dealing with wing flutter the following are to be mentioned:

Theoretical studies:

Theodorsen, Th., *General Theory of Aerodynamic Instability and the Mechanism of Flutter*, N.A.C.A. Technical Report No. 496, 1935.

Kassner, R., and Fingado, H., *The Two-Dimensional Problem of Wing Flutter*, Luftfahrtforschung, Vol. 13, No. 11, 1936. Translated in Journal of the Royal Aeronautical Society, Vol. 41, pages 921–944, October, 1937.

Lombard, A. E., *Thesis on Wing Flutter*, California Institute of Technology, 1939.

Bergen, W. B., and Arnold, L., *Graphical Solution of the Bending-Aileron Case of Flutter*, Journal of the Aeronautical Sciences, Vol. 7, No. 12, page 495, October, 1940.

Experimental studies:

Studer, H. L., *Experimentelle Untersuchungen über Flügelschwingungen*, Mitteilungen aus dem Institut für Aerodynamik der Technischen Hochschule Zürich, No. 4, 1936.

Rauscher, M., *Model Experiments on Flutter at the Massachusetts Institute of Technology*, Journal of the Aeronautical Sciences, Vol. 3, No. 5, page 171, March, 1936. Also in Aviation, January, February, April, May, 1936.

Voigt, H., *Wind Tunnel Investigations of Torsion-Bending Type of Wing Flutter*, Luftfahrtforschung, Vol. 14, No. 9, pages 427–433, 1937. Translated in N.A.C.A. Technical Memorandum No. 877, 1938.

Cicala, P., *Comparison of Theory with Experiment in the Phenomenon of Wing Flutter*, l'Aerotecnica, Vol. XVIII, No. 4, April, 1938. Translated as N.A.C.A. Technical Memorandum No. 887, 1939.

The Proportioning of Aircraft Frameworks

N. J. HOFF*

Polytechnic Institute of Brooklyn

SUMMARY

A routine procedure, consisting of three steps, is presented for calculating the stresses in and the stability of plane frameworks. In the first step the preliminary sizes and gages of the bars are chosen upon tentative assumptions for the end-fixity. In the second, the assumptions made are checked by rational approximate methods. In the third and last, the final check of both stresses and stability is obtained in a single step by the use of James's version of the Hardy Cross method of moment distribution. It is suggested that the procedure here described be denoted the Lundquist-Stanford method of proportioning frameworks as distinct from the Lundquist method of determining critical loads.

INTRODUCTION

THE PROPORTIONING of the bars of frameworks involves two different tasks: It must be shown that the maximum stresses caused by all external loads are less than the allowable stresses for the material used, and that the axial forces in the bars are smaller than their first critical values (buckling, often Euler loads). These two problems are independent since it is known that the formulas of the theory of elasticity may yield stresses well below the allowable limits in cases where the external loads are higher than the buckling loads. The method suggested in the present paper tackles both tasks simultaneously, is believed to be simple enough for routine work and eliminates two major inconsistencies often encountered in aircraft design.

One of these is the assumption of a constant restraint coefficient for all bars. This obviously cannot correspond to reality since the restraining effect of the joints against rotation of the ends of a compressed bar depends upon the number and the sizes of the bars attached to the joints, and upon the axial forces acting in them. This effect can vary widely even for the same bar for different conditions of loading of the framework, and the assumption of a single constant value for all bars and all loading conditions is entirely unwarranted and leads to structures of very unequal strength.

The second inconsistency is to neglect the bending stresses caused by transverse loads, such as seats, control devices, dashboards, etc., applied to the bars between the joints. Occasionally stress departments establish the sizes and gages of the bars with no regard to side loads and the accessories are fixed later in the shop without checking the stresses caused. Such a procedure is absolutely not permissible.

As regards the actual calculations, methods for determining the axial forces in frameworks have long been developed. The calculation of the bending moment distribution due to lateral loads, or external moments, has been made an easy task by James's adaptation of Hardy Cross's method of moment distribution.[1] The possibility of using this method for determining the critical loads of a framework was detected and developed by Lundquist.[2] A simpler criterion, based on the convergence properties of the Hardy Cross method was published by the author in a recent issue of the Journal of the Aeronautical Sciences.[3, 4] The use of this criterion for checking both the stresses and the instability is the main feature of the method suggested here.

OUTLINE OF THE METHOD

The present method of proportioning the bars in a plane framework consists of three distinct steps. In the first the sizes and gages of the bars are chosen upon arbitrarily assumed values of the coefficients of end-restraint. In the second, this choice is refined by checking the assumed values by approximate but rational methods, and by changing the sizes and gages to obtain a structure of sensibly uniform strength. In the third step a final check of the moment distribution and of the stability is obtained by the use of the Hardy Cross method.

It must be borne in mind that the third step alone suffices for checking the bending stresses as well as the buckling loads. The two preliminary steps, therefore, need not be undertaken in a too detailed and careful way. Nevertheless, they are useful due to the circumstance that the moment distribution method is not well suited for the preliminary steps of proportioning, since it does not give much indication which members should best be strengthened if the framework is found to be unstable. Also, the work involved in a complete moment distribution analysis is greater than is justified, when, in the first stages of proportioning, sizes of members are repeatedly changed.

THE PREPARATORY STEP

Before proceeding to the method proper some preparatory work must be carried out. First the form of the framework has to be decided upon. Then the axial forces must be determined in all bars and for all load-

Presented at the Structures session, Ninth Annual Meeting, I.Ae.S., New York, January 30, 1941.

* The major part of this paper was written while the author was at Stanford University. He acknowledges his indebtedness to Prof. A. S. Niles for his criticisms, and to Mr. W. J. Abokair for having drawn the diagrams.

ing conditions. It is convenient to prepare separate line drawings of the framework for each loading condition and to write the axial forces above the lines representing the bars. An additional diagram should show the maximum forces in the bars, and the few bars, if any, in which failure will be caused by tension, can immediately be proportioned.

First Step—Rough Proportioning

The simplest start, when choosing the preliminary sizes and gages of the bars in compression, is to assume a constant restraint coefficient of 2. Even at this stage of the work, however, it is preferable to assume different values for the different bars in order to avoid too many changes later. It is well to discriminate between chord and bracing members, between bars, the ends of which are attached to predominantly tension members or lightly loaded compression members, or mainly to highly loaded compression members. Also, it should be borne in mind that for uniformity in the case of chord members the same size and gage is usually carried through several bays, though the forces in the different bays are different. Thus part of the bar is relatively strong, part relatively weak. Furthermore, it is of importance to realize that bracing members are generally of smaller size than the chord members and restrain the latter to a smaller degree than *vice versa*. The actual restraint coefficient for longitudinals often will be found less than 2, infrequently even near unity; that for bracing members mostly more than 2, sometimes even not far from 4.

The procedure of selecting the right sizes and gages with the aid of column charts or column formulas on the above outlined choice of the restraint coefficients is basically very simple. It is, however, somewhat complicated by the circumstance that the highest loads in the different bars are caused by different loading conditions of the framework. Therefore, the maximum loads for each bar should be taken from the line-drawing of the framework showing the maximum axial forces, but the restraining effect of the adjacent bars should be taken into account by considering the loads in them as shown by the line-drawing of the corresponding loading condition.

The simplest way to proportion bars loaded laterally is to assume simple supports at the ends and to neglect the influence of the axial forces upon the bending moments. It is known that the end-restraint may materially reduce the maximum moments, especially if the loads are applied near the ends of the bar, whereas compressive axial forces may very much increase them, particularly if the load is applied near the middle of the bar. For more detailed information on the effect of end-restraint upon the maximum bending moments a previous paper[5] by the author may be helpful. The influence of the axial load can be calculated by Perry's formula with very good accuracy for the purposes of preliminary proportioning:

$$M = M_0 \frac{P_E}{P_E - P} \tag{1}$$

where M_0 is the maximum bending moment without axial force but with due regard to end-fixity, P_E the column load of the bar and P the actual compressive force in the bar.

Second Step—Refinement of the Proportioning

The second step is conveniently started by calculating the ratios L/j for every bar where L is the length of the bar and

$$j = \sqrt{E'I/P} \tag{2}$$

with E' the effective modulus of elasticity,[6] I the moment of inertia of the cross-section and P the axial force acting in the bar. These ratios will be found smaller than 2π provided that no error was made in the first step. $L/j > 2\pi$ means namely that the bar would be unstable even if both its ends were rigidly fixed. This corresponds to the assumption of a restraint coefficient greater than 4.

Then the stiffnesses S of the bars have to be determined assuming the far ends to be rigidly fixed. For this purpose Lundquist's tables[7] should be used. By summing up the stiffnesses of all bars attached to any joint the stiffness ΣS of the joint itself against twisting is obtained. This should always be positive. A negative value means that the joint would not resist twisting even if the far ends of all bars common to it were rigidly fixed. Since the actual constraint is always less, such a joint is evidently unstable.

It should be borne in mind that both above stipulations are minimum requirements. Failure to comply with them is equivalent to instability. On the other hand their fulfilment is not a sufficient criterion of stability. Hence some further calculations are necessary.

It is suggested, therefore, to subdivide the framework into groups of bars by inserting imaginary pin-joints between the groups and by considering the bars contained in the same group to be rigidly fixed to each other. The subdivision has to be undertaken in such a way as to attach the greatest possible number of bars in tension, or slight compression, to each bar which is heavily loaded in compression. In this context "heavily loaded" means any compression bar having an L/j ratio greater than π. These bars will be called the principal bars of the groups. Obviously they are unstable without some end-constraint. On the other hand, they may be strong enough if the elastic restraining effect of the other bars in the group is taken into account. This can easily be done with the aid of the relative stiffness factor method developed by the author in a previous publication.[8] According to this, the stiffnesses ΣS of the joints at the ends of the principal bar must be calculated by summing up the stiffnesses of

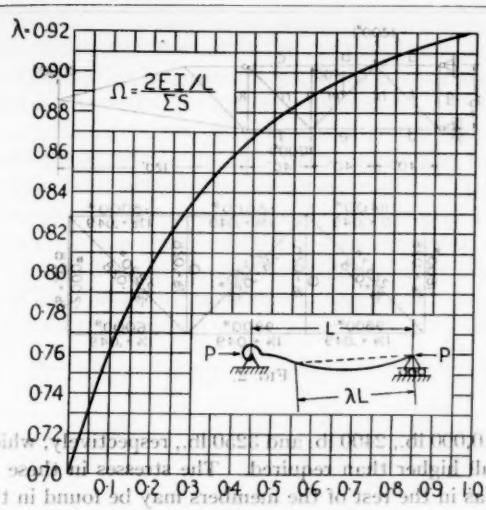

FIG. 1.

all bars common to them but disregarding the stiffness of the principal bar itself. In the groups the far ends of most of the bars will be assumed to be pinned. For such the stiffness factors for pinned far end must be taken from Lundquist's tables. If they are not pinned, some value between those for pinned and for fixed end should be chosen. The ratio of the value $2E'I/L$ for the principal bar to the stiffness of the joint is a non-dimensional parameter and is called the relative stiffness factor, Ω:

$$\Omega = 2(E'I/L)/(\Sigma S) \quad (3)$$

The effect of the elastic restraint at the ends of the bar is to change the deflected shape at buckling and to cause inflection points to appear. The location of these inflection points is determined by the relative stiffness factors. On the other hand, the buckling load of an elastically restrained bar is equal to the buckling load of a simple (non-restrained) bar of a length equal to the distance between the points of inflection. Thus, the buckling load can easily be calculated if the relative stiffness factors at the ends of the bar are known. Results of such calculations were presented in the form of charts in the paper mentioned. In these a factor λ, by which the length of a column must be multiplied in order to obtain the length of the equivalent non-restrained column, is plotted against the relative stiffness factors Ω. One of these charts will be needed in the calculations of the numerical example and it is reproduced as Fig. 1.

After the relative stiffness factors for both ends of the principal bars have been computed and the equivalent length coefficients λ taken from Fig. 1, the load which can be sustained by the elastically restrained principal bar of length L can be calculated from the formula:

$$P_{cr} = \pi^2 E'I/(\lambda L)^2 \quad (4)$$

where E' is the effective modulus of elasticity.[6]

If the framework has been completely subdivided into groups of bars for each loading condition independently, and in all these cases every principal bar, or in other words every group, has been found to be stable, then the entire framework is in stable equilibrium. Moreover, it is stronger than required since it would be stable even if the imaginary pins were real. Therefore, this requirement is sufficient but not necessary for stability contrary to the two requirements stated at the beginning of this section. Since, further, the final check of the stability of the whole framework will be obtained in a more convenient way in the third step, it is not necessary to carry out the second step too rigorously. Provided some experience with the method has been acquired, it is sufficient to select only a few bars for principal bars and to check their stability in groups which contain some of the adjacent bars only.

Furthermore, it is convenient to regard the bars carrying lateral loads as principal bars when subdividing the framework into groups. The stiffnesses of the joints at their ends must be calculated in exactly the same way as in the case of buckling. Then the fixed-end moments of the principal bar have to be determined. For the most important case of a concentrated load the fixed-end moments have been computed and graphically represented in James's paper, and may be found in Niles's and Newell's textbook.[9]

The real distribution of the end moments in the isolated system consisting of a principal bar and of the two elastically restrained joints at its ends can next be obtained by the Cross method. Alternately the two joints are released, balanced, the unbalanced moment distributed between the elastic joint and the principal bar, and the carry-over moment applied at the other end of the principal bar. After the final end moments have been obtained the resulting moment diagram can be determined by superimposing the moment diagrams for the side load and for the two end moments. All three are represented by curves rather than straight lines due to the effect of the compressive force. These curves can be calculated from standard formulas given in textbooks.[10]

THIRD STEP—FINAL CHECK

After the sizes and gages of all bars have been chosen in the first and second steps, the moment distribution in the entire framework must be calculated. First the fixed-end moments are determined as explained above. Then the usual routine procedure of the Cross method is carried out with the aid of Lundquist's values for the stiffness and carry-over factors. The present author proved that if by this procedure finite values of the end moments are obtained, or in other words, if the moments to be balanced tend to decrease in successive steps and, therefore, the moment distribution method is convergent, then the entire framework is in stable equilibrium. If, however, the moments to be balanced tend

to increase in successive steps, or in other words the method is divergent and no finite values for the end moments can be obtained, then the framework is unstable.

If the framework is found to be unstable, some of the bars must be reinforced. The methods outlined in the second step are useful in indicating which bars may best be reinforced. If after this change the procedure of the Cross method becomes convergent, the stability is established. Then the maximum combined stresses must be calculated from the maximum bending stresses and the compressive stresses. It should not be overlooked that bending stresses are not confined to the laterally loaded bars but prevail in all other bars too. They can be dangerous, especially in compression bars adjacent to the laterally loaded bars.

It must be mentioned, however, that in certain particular cases the moment distribution method can be convergent though the structure is not stable. Such cases can be detected by changing the order of balancing. Then either the procedure becomes divergent, or if finite values are again obtained for the end moments, they are different from those first obtained. On the other hand, if the framework is in stable equilibrium the moment distribution is independent of the order of balancing. Although such particular cases are very unlikely to occur, they should be understood. They have been discussed by the author in previous papers.[3, 4]

Numerical Example

The example has been chosen so as to be representative of the conditions prevailing in the middle portion of the side panel of a welded steel airplane fuselage. With a view to eliminate unnecessarily lengthy calculations, the right end carrying the external load is replaced by a structure attached by ideal pin joints to the part comprising three bays to be investigated. The left end is assumed simply supported, as indicated in Fig. 2. The tensions in the members can be calculated by any routine procedure after the load of 400 lb. applied at the middle of bar m has been replaced by the statically equivalent forces of 200 lb. at the joints at the ends of the bar. The tensions so obtained are indicated in Fig. 2.

For a first proportioning the end-fixity coefficient is tentatively assumed 1.5 for the chord members, 2 for the vertical bracing member at the left and 3 at the right. Since the equivalent length L' of a bar is given by

$$L' = L/\sqrt{C} \qquad (5)$$

where L is the actual length of the member and C the end-fixity coefficient, the equivalent lengths of the aforementioned bars are found to be 32.6 in., 28.3 in. and 23.1 in., respectively. The necessary sizes and gages of the tubes have been chosen with the aid of the charts[11] reproduced in ANC-5 and are indicated in Fig. 2. The column strength of bars a, b, g and k is 11,800

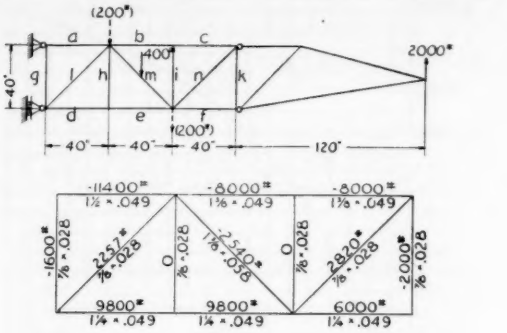

Fig. 2.

lb., 10,000 lb., 2400 lb. and 3250 lb., respectively, which are all higher than required. The stresses in these as well as in the rest of the members may be found in the attached table. The sizes of the members of the tension chord and of the bracing members are chosen greater than required by the present loading condition in order to obtain a structure more representative of actual aircraft.

A rough estimate of the maximum bending moment in bar m can be reached by assuming its left end simply supported and its right end rigidly fixed, since the highly loaded compression chord at its left end can exert but very little restraint, whereas the tension members at its right end are relatively stiff. The effect of the longitudinal component of the force of 400 lb. applied at the middle of the bar is neglected. Its transverse component of 282 lb. causes, under the assumed conditions, a maximum bending moment of 3000 in.lb. Assuming tentatively that the column strength of the bar is twice the compressive force acting in it, Perry's formula (Eq. 1) yields $M_{max.} = 6000$ in.lb. On these assumptions the tentative choice of the size of bar m was made as shown in the table.

For the calculations of the second step the stiffnesses of the bars are required. These are, however, influenced by the stresses, since as soon as they exceed the proportional limit, an effective modulus of elasticity E' must be used instead of Young's modulus E. The effective modulus of each bar was calculated from Fig. 4-2 of ANC-5 in accordance with the suggestions of section 1.512 of the same publication.[11] With the aid of these values the bending stiffness $E'I$, the value of $j = \sqrt{E'I/P}$ and the ratio L/j were computed. The values of the stiffness factor were taken from Lundquist's tables[7] and multiplied by 4 to conform with Hardy Cross's original definition. The result is tabulated under the heading $SL/E'I$.

After that the framework was subdivided into groups of bars as shown in Fig. 3. In this particular case one end of each heavily loaded bar is pinned, the other end rigidly attached to one, and in the case of bar m to two, tension members. The stiffness of the joint in torsion is, therefore, simply the stiffness of the tension member

in bending. In the present case, however, this must be calculated with the aid of the stiffness factor for "far end pinned" in Lundquist's tables. The corresponding (fourfold) values are listed in column S''. The relative stiffness factor was calculated according to the definition given above and the corresponding equivalent length coefficient λ taken from Fig. 1. Then the equivalent length L' was calculated and the critical load taken from the charts of ANC-5. A comparison of the critical loads P_{cr} so obtained with the tensions P shows that bars a and k are unstable and bars b and c very near the critical condition. Since, however, it is hoped that

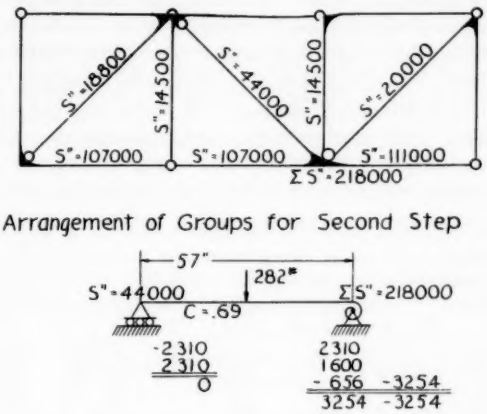

FIG. 3. Moment distribution method applied to bar m.

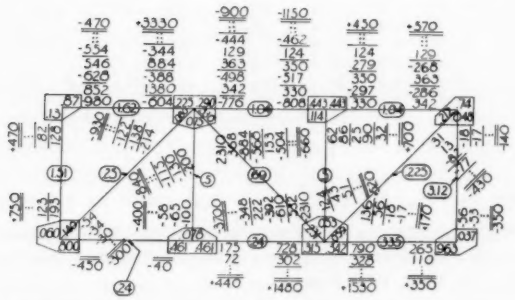

FIG. 4. Moment distribution analysis; carry-over factors in circles; distribution factors in polygons.

the restraint discarded by introducing the pin joints will suffice for stability, the originally chosen sizes of the bars are retained for the calculations of the final step.

Before starting this, however, the stresses in bar m must be checked. The fixed-end moment is given by the formula

$$M_A = M_B = c_A WL/8 \qquad (6)$$

where M_A and M_B are the end moments, W is the transverse load, L the length of the bar and c_A, a coefficient dependent upon L/j. In the present case $c_A = 1.15$ according to Niles and Newell.[9] Hence, the fixed-end moment is 2310 in.lb. The procedure of the moment distribution is shown in Fig. 3. The maximum bending moment is found by drawing a moment diagram. Since this is very similar to the final one shown in Fig. 6, it is omitted here. The maximum stress caused by simultaneous bending and compression was found to be well within the allowable limits.

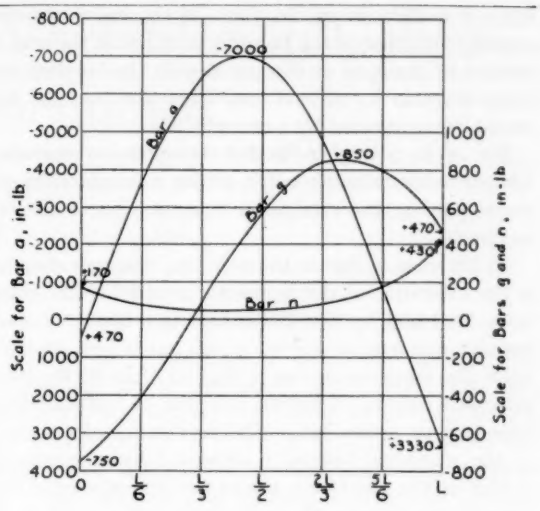

FIG. 5. Moment diagrams of bars a, g and n.

The calculations of the final check by the moment distribution method are shown in Fig. 4. By this the structure is found to be stable since the end moments converge toward limiting values, though very slowly. Slow convergence, however, is to be expected since the structure is extremely near instability. In Fig. 4 the greater part of the steps is omitted for lack of space and the final results are given in round numbers.

In Figs. 5 and 6 final moment diagrams of four bars are given. The curves were calculated by the formulas of the textbooks mentioned above.[10]

Bar n is in tension and the influence of the tensile

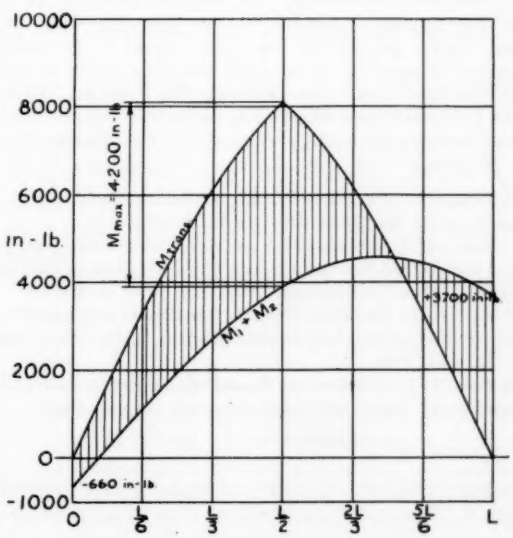

FIG. 6. Moment diagram of bar m.

force is evident from the form of the curve showing a great reduction of the bending moment in the middle portion of the span as compared with the bending moment diagram for no end load when the two end moments are connected by a straight line.

Bar *g* is a highly loaded compression member. Therefore its moment curve shows a considerable increase against the straight line connection of the end moments.

In the case of bar *m* the resulting moment diagram is the difference of the moments caused by the transverse load and by the end moments. Since the compressive end load acting upon this bar is less, its effect upon the moment curves is slighter than in the cases discussed before. Nevertheless, the curvature of the lines is very noticeable. The very material reduction of the maximum moment, caused by the elastic restraint at the right end, shows the importance of considering the framework as a whole rather than to assume pin joints between its members. Further, it is interesting to note that the sign of the end moment at the left is opposite to that at the right. This indicates that bar *m* helps to stabilize bar *a* rather than profiting from any restraining effect at the left support.

The right end of bar *a* rotates considerably due to the transverse load acting upon *m*. The deflections of bar *a* so caused give rise to important bending moments due to the high compressive axial load. These bending moments tend to increase the deflections, but after a certain value further deflections are resisted by the stiffness of bars *m* and *g*. This is manifested by the appearance of inflection points in the distorted shape of the bar corresponding to the location of the zero-moment near the ends. Therefore, the end moments in this case represent elastic restraints rather than external loads and have signs opposite to that of the maximum moment. Nevertheless, the maximum bending moment is extremely high and well above the allowable values. This circumstance again proves the necessity of checking frameworks as a whole, since in this case the transverse load causes much higher moments in bar *a* than in bar *m* upon which it is directly acting.

Bar	P, Lb.	Tube	A, In.^{2}	ρ, In.	f_c, Lb./In.^{2}	$10^{-6}E'$, Lb./In.^{2}	$j=\sqrt{E'I/P}$, In.	L/j	$SL/E'I$	$10^{-3}S$, In.Lb.	$10^{-3}S''$, In.Lb.	Ω	λ	L', In.	P_{cr}, Lb.
a	−11,400	1½ × .049	.2230	.513	−51,000	23.2	10.90	3.7	1.7	58	...	3.6	.95	38	10,300
b	− 8,000	1⅜ × .049	.2040	.469	−39,200	28.0	12.50	3.2	2.4	75	...	4.3	.95	38	8,400
c	− 8,000	1⅜ × .049	.2040	.469	−39,200	28.0	12.50	3.2	2.4	75	...	4.3	.95	38	8,400
d	9,800	1¼ × .049	.1840	.425	53,200	22.2	8.65	4.6	6.3	116	107	...	..	..	....
e	9,800	1¼ × .049	.1840	.425	53,200	22.2	8.65	4.6	6.3	116	107	...	...	...	...
f	6,000	1¼ × .049	.1840	.425	32,700	29.0	12.7	3.15	5.2	126	111	...	...	...	...
g	−1,600	⅞ × .028	.0745	.299	−21,400	29.0	11.0	3.64	1.8	8.7	...	.09	.755	30.2	2,100
h	0	⅞ × .028	.0745	.299	0	29.0	...	0	4.0	19.4	14.5	...	..	..	....
i	0	⅞ × .028	.0745	.299	0	29.0	...	0	4.0	19.4	14.5	...	..	..	....
k	−2,000	⅞ × .028	.0745	.299	−26,800	29.0	9.8	4.08	1.0	4.85	...	.485	.874	35	1,550
l	2,257	⅞ × .028	.0745	.299	30,300	29.0	9.25	4.32	6.0	20.4	18.8	...	..	..	....
m	− 2,540	1⅜ × .058	.240	.466	−10,600	29.0	24.4	2.34	3.2	85	44	.24	.82	46.7	6,850
n	2,820	⅞ × .028	.0745	.299	37,900	28.3	8.20	4.9	6.5	21.7	20	...	..	..	....

Bars *a* to *k* are 40 inches long, *l* through *n* are 57 in.

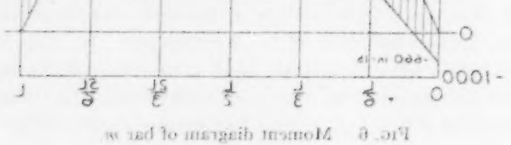

References

[1] Niles, A. S., and Newell, J. S., *Airplane Structures*, 2nd edition, Vol. II, page 36, John Wiley and Sons, New York, 1938; Cross, Hardy, *Analysis of Continuous Frames by Distributing Fixed End Moments*, Proceedings A.S.C.E., Part I, Vol. 56, No. 5, page 919, May, 1930; and James, B. W., *Principal Effects of Axial Load on Moment Distribution Analysis of Rigid Structures*, Thesis, Stanford University, 1933, and N.A.C.A. Technical Note No. 534, 1935.

[2] Lundquist, E. E., *Stability of Structural Members Under Axial Load*, N.A.C.A. Technical Note No. 617, 1937.

[3] Hoff, N. J., *Instability of Aircraft Frameworks*, presented at the 2nd Annual Summer Meeting of the Institute of the Aeronautical Sciences at Pasadena, California, June 24, 1940.

[4] Hoff, N. J., *Stable and Unstable Equilibrium of Plane Frameworks*, Journal of the Aeronautical Sciences, Vol. 8, No. 3, page 115, January, 1941.

[5] Hoff, N. J., *Transversely Loaded Framework Members*, The Journal of the Royal Aeronautical Society, August, 1935.

[6] von Kármán, Th., Forschungsarbeiten, No. 81, 1910, Berlin; see also Timoshenko, S., *Theory of Elastic Stability*, McGraw-Hill, New York, 1936, page 45.

[7] Lundquist, E. E., and Kroll, W. D., *Tables of Stiffness and Carry-Over Factor for Structural Members Under Axial Load*, N.A.C.A. Technical Note No. 652, 1938; also page 146 of Niles's and Newell's textbook on *Airplane Structures*, Reference 1 above.

[8] Hoff, N. J., *Elastically Encastred Struts*, The Journal of the Royal Aeronautical Society, Vol. XL, No. 300, page 663, September, 1936.

[9] See page 123 of Niles's and Newell's textbook on *Airplane Structures*, Reference 1 above.

[10] Chapter I of Timoshenko's textbook on *Theory of Elastic Stability*, Reference 6, above, and page 65 of Niles's and Newell's textbook on *Airplane Structures*, Reference 1 above.

[11] Army-Navy-Civil Committee on Aircraft Requirements, ANC-5 *Strength of Aircraft Elements*, January, 1938, Figs. 4–5 to Figs. 4–9.

The Effect of Design Variables on Cargo Plane Performance

ADOLPH BURSTEIN
Stinson Division, Vultee Aircraft, Inc.

ABSTRACT

The possible development of an air freight system in the United States brings up the relationship of aerodynamic design to the economical operation of cargo planes. It is shown that a careful analysis, in the light of operating costs and safety of all factors entering the design of an airplane is essential, if a sound design is to be evolved.

A method of evaluating the major design variables is presented. It is also shown that the operation of the plane and the degree of safety desired must be decided upon before proceeding with a design.

Because of the broad scope of the investigation, the results presented should be considered qualitatively only. However, definite trends are indicated. No fundamental aerodynamic difference exists between a well-designed cargo plane and a passenger plane.

INTRODUCTION

IN RECENT MONTHS air freight has received considerable publicity as the coming development in airline transportation. The success of this operation is predicated on drastic reductions in tariffs. Tariffs that are a fraction of the present air express charges may be possible with the operation of special planes, used solely for transportation of goods.

Assuming that there is demand and volume for air freight operation, it becomes the task of aeronautical engineers to prove that cargo planes can be designed to operate economically enough for the projected service, and to select the most suitable design. The configuration of a plane is the result of proper evaluation of major aerodynamic variables with respect to economy and safety. The items that must be first considered are:

Gross weight
Wing aspect ratio
Wing loading
Power loading
Number of engines
Percentage of power for cruising.

It is obvious that the number of possible combinations of the above is legion, and simplified assumptions must be made in order to keep the work within reasonable limits.

Presented at the Air Transport session, Ninth Annual Meeting, I.Ae.S., New York, January 30, 1941.

ASSUMPTIONS

Due to the limitations of space, the basis for the calculations can be discussed only briefly. The data used are based, whenever possible, on existing designs and information to be found in N.A.C.A. Reports and aeronautical literature. No unconventional features are considered, and it is believed that no over optimistic assumptions have been made.

The drag of the airplane is broken down into major components as follows:

N.A.C.A. 23012 section was used for the wings and the drag increased by 20 per cent to allow for manufacturing imperfections. (Refs. 1 and 2.) For simplicity, elliptical lift distribution was assumed for the determination of induced drag.

The empennage drag was taken to vary with that of the wing, and the tail area assumed to follow the expression:

$$\frac{S_T}{S_W} = C_1 + C_2(W/S)$$

The resistance of the nacelles is composed of that due to the basic nacelle drag plus that due to cooling. From page 9 of reference 3 and Table XI of reference 4,

$$C_{D_{nacelle}} = 0.38 \times 0.1193 = 0.045 \text{ for } \alpha_{incidence} = 0°$$

based on nacelle frontal area which was computed for 56 inches nacelle diameter.

The cooling drag was determined by the method of reference 3 considering adjustable cowl flaps and using 6 inches and 4 inches H_2O baffle pressure drop for level and climbing flight, respectively. Planes up to 40,000 lbs. gross weight were taken to be in the twin-engine class, and all others fell in the four-engine category.

The remainder of the drag is lumped together as fuselage plus interference. The variation of this item with gross weight can be shown to follow the expression

$$SD_{F+I} = 9.5\left(\frac{W}{25{,}000}\right)^{0.8}$$

This is based on a modern transport, and the variations of cross-section with payload and Reynolds Number are considered. It is further supposed that the in-

cidence is set for the particular cruising condition, keeping parasite drag at a minimum.

Instead of trying to fit the nearest existing engine to the various powers required for the combinations, an infinite variety of power plants was supposed to exist. Straight line variations of propeller r.p.m. and diameter were estimated for the complete range, using 2400 METO* Power as the upper limit of available engines.

Propeller diameters were selected using information in reference 5. The propellers were also checked for tip speed effects. Only at take-off were the tip speeds critical.

Since the propellers could be designed for cruising conditions selected, $\eta = 82$ per cent was assumed for cruising at 65 per cent METO Power. This same efficiency was used in determining the parasite drag of existing airplanes.

Performance Calculations

The performance of a cargo plane is important from two aspects, economical transportation of goods and safety. The former is inherent in the relationship of cruising speed to payload and operating cost, while the latter is best expressed in terms of one-engine-inoperative climb and take-off. Landing over an obstacle is another important criterion of safety. However, only the deceleration runs were computed.

Conventional methods of performance estimation were employed and require no particular elaboration. The one-engine-inoperative climb at sea level was computed assuming fully feathered propeller for the inoperative engine, while the remaining engines were delivering METO Power. The method given in reference 6 was closely followed, taking into account the additional drag due to unsymmetrical thrust. The values of the resistance of the feathered 3-bladed propeller were kindly supplied by the Hamilton Standard Propeller Company.

The take-off criteria adopted were in line with Amendment 56 of the C.A.R. prescribing alternate requirements for scheduled airline operation. It is possible that these regulations were not set up with a strictly cargo operation in view, and that the operators of cargo planes in the future will request a liberalization of the requirements, which may be granted. Such a change would be of particular benefit to twin-engine craft; the four-engine planes would not show an appreciable gain in economy.

The present calculations are based on safe operations from a 3500 ft. take-off surface at sea-level. Assuming that one engine fails at the point of "unstick," the pilot should have the choice of either throttling the remaining engines and coming to rest within the above boundary, or else proceed to climb and reach a 50 ft. altitude above the take-off surface within 3500 ft. from the start. Because of the shortness of time available to the pilot, the landing gear is considered extended and the inoperative propeller in low pitch. The functioning engines are assumed to deliver take-off power. The speed at take-off is that required to maintain control, as pointed out by Johnson in reference 7.

Take-off run was computed using the method given in reference 8, allowing 2 per cent for correction. It was decided that the transition stage can be safely omitted, since the climb was assumed to be at take-off speed. Results found in reference 9 indicate the correctness of the above conclusion Then, the distance to clear a 50 ft. obstacle is given by

$$S = \frac{V_T^2 W}{63 T_e} + \frac{50W}{T_F} = \text{Ft}$$

where V_T = take-off speed
W = gross weight
T_e = excess thrust at $0.71 V_T$
T_F = excess thrust at V_T

The deceleration run was computed from the well known equation

$$L_G = \frac{0.033 W V_T^2}{\mu' W - D} \log_e \left[\frac{\mu' W}{D}\right] = \text{Ft.}$$

where μ' = ground friction coefficient = 0.30
D = air drag of the airplane at V_T

Payload

Payload being the reason for the existence of the plane, plays a vital part in the evaluation of any design. However, it does not form the sole criterion.

Weight empty determination was based on existing data for past designs. The effect of the variables on the structural weight was taken into account, and proper allowance was made for equipment, furnishings and flooring required to handle cargo. All-metal type of construction was assumed.

Two- or three-men crews were assigned to handle twin- and four-engine planes, respectively.

Not only the fuel-and-oil load, but the entire operating cost is tied up with the operating range. Since the primary concern of the investigation was to compare the various designs, only one flight leg is chosen. A two-hundred-mile flight leg was picked, as it appeared to fit most closely the initial operation of cargo planes. Enough fuel and oil, then, is carried on board to meet the following requirements,

Length of trip	200 miles
Distance to alternate field	200 miles
Average headwind (including allowance for circling and climb)	10 m.p.h.
Maneuvering on the ground	0.12 hr.
Reserve fuel for	1.00 hr.
Oil weight	$^1/_{10}$ fuel weight
Cruising altitude	10,000 ft.

Block-to-block speed and fuel load are based on the above.

*A Maximum Except Take Off.

Operating Cost

No discussion of cargo planes can be made without introducing operating cost, at least as a yardstick. Briefly, the cost of transporting goods by air consists of three major items—direct flying costs, indirect flying costs or airline overhead, and pick-up and delivery charges, including advertising and solicitation. Since the first item is most directly dependent on airplane design, and the others are very difficult to estimate without special study, it was the only one considered.

Direct flying costs are chargeable to:

Crew
Fuel and oil
Maintenance
Depreciation
Insurance.

It is felt that the values used closely approximate present-day airline experience. Some of the items were taken from reference 10. The initial cost, which determines depreciation charges, was arranged in such a way as to reflect the effects of various designs.

In order to be conservative, the engines and propellers were assumed to depreciate in 5000 hours, and the airplane bare was depreciated over a period of five years at a utilization of 2000 hours a year. Zero salvage value was considered.

Maintenance costs were based on the following expressions:

Airplane maintenance cost (\$/hr.) = 0.000458 (Weight airplane bare)
Engine maintenance cost (\$/hr.) = $0.0044P$ (%P used)

No claim is made that the costs as used are absolutely correct; however, their consistent application serves the purpose of bringing out the relative merits of various designs. For the same reason 100 per cent load factor is used throughout, although a load factor in excess of 65 per cent would not allow properly for peak loads.

Discussion of Results

Before going into the actual selection of a cargo plane design, the effects of the variables on performance enumerated earlier will be illustrated by means of graphs. Only representative graphs are singled out for the discussion.

Cruising Speed

Fig. 1 was selected to illustrate the effect of the design variables on cruising speed of 55,000 lb. plane operated at 65 per cent power at 10,000 ft. Obviously the speed increases as power loading decreases. These curves also indicate that for each power loading there is an optimum wing loading, and increasing the wing loading beyond this point results only in loss of speed. This effect is even more pronounced for the airplanes

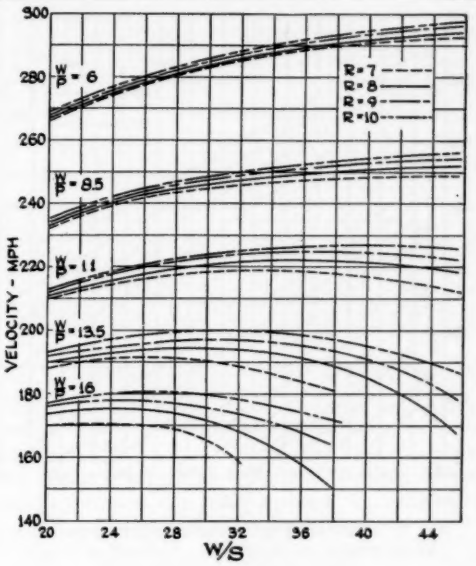

Fig. 1. Cruising speed.
Gross weight = 55,000 lbs., 65 per cent power.
Altitude = 10,000 ft.

cruising at 45 per cent power, not shown here. It is also interesting to note the pronounced effect of aspect ratio on speed at higher power loading; up to 20 m.p.h. may be gained by going from aspect ratio of 7 to 10. An anticipated increase of speed with gross weight is brought out in Fig. 2. The dotted lines indicate the change from two-engine to four-engine craft.

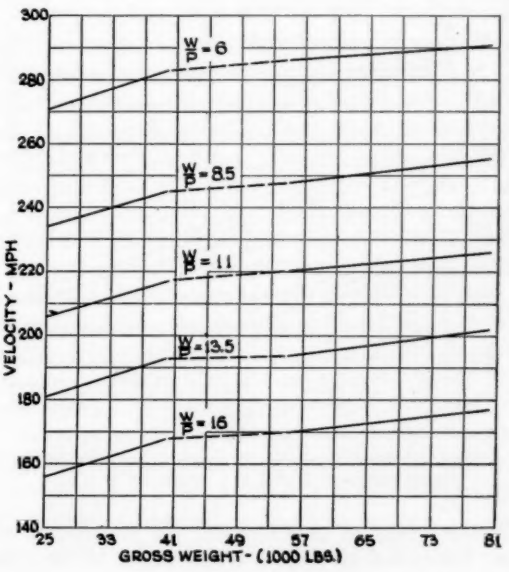

Fig. 2. Cruising speed.
w/s = 32, R = 8, 65 per cent power.

One-Engine-Inoperative Climb

Figs. 3 and 4 indicate the sharp decrease of the one-

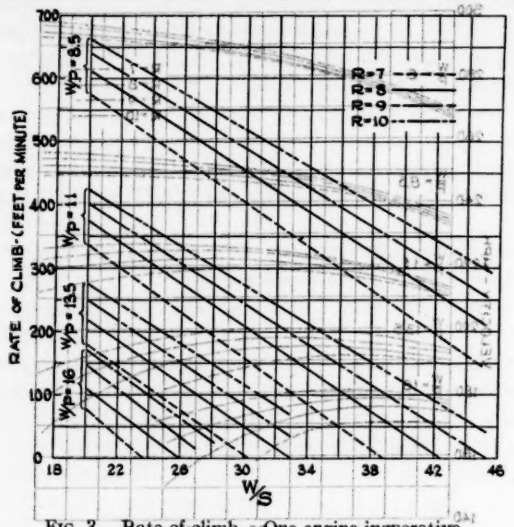

FIG. 3. Rate of climb. One engine inoperative. Gross weight = 40,000 lbs. Altitude = S.L.

engine-inoperative climb rate with increased wing loading for constant power loading. Here again the effect of aspect ratio is very pronounced, particularly in Fig. 3, which represents a twin-engine airplane.

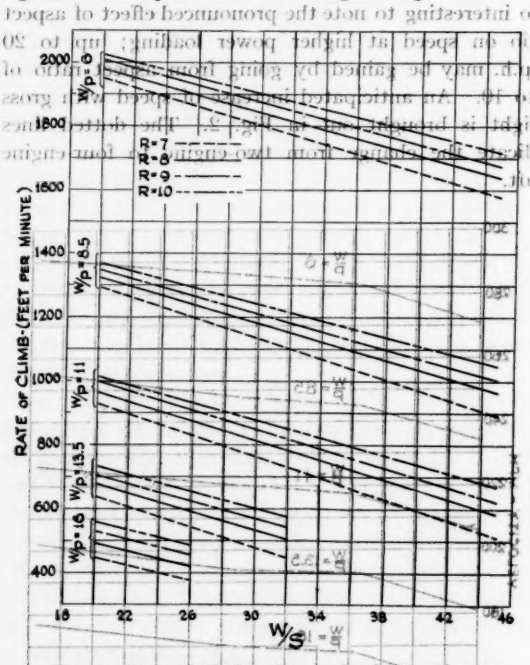

FIG. 4. Rate of climb. One engine inoperative. Gross weight = 55,000 lbs. Altitude = S.L.

In this phase of performance, the four-engine airplane illustrated on Fig. 4 is far ahead of the twin-engine plane, as the following example will illustrate. From Fig. 4, a plane of 13.5 lbs./hp. power loading, 32 lbs./ft.^{2} wing loading and aspect ratio of 10 has a climb of 580 ft./min. In order to have the same performance in a twin-engine airplane of the same aspect ratio, a power loading of 8.5 lbs./hp. and a wing loading of 26 lbs./ft.^{2} must be employed. This is an increase of 59 per cent in power, and an increase of 23 per cent in wing area.

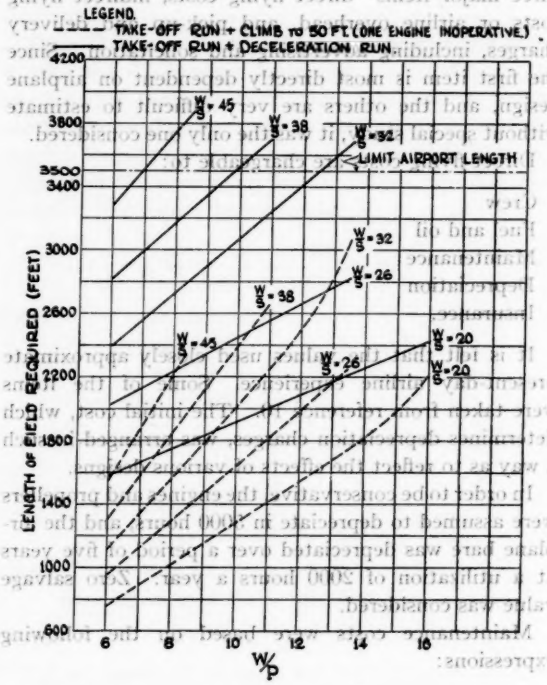

FIG. 5. Required airport length at sea level. Gross weight = 55,000 lbs. Aspect ratio = 10. 4 engines.

Airport Length Required

Emergency take-off criteria discussed before resolve themselves into the length of airport required for safe operation of any particular design. Representative curves for a four-engine plane are shown on Fig. 5. Only aspect ratio of 10 is shown. The solid lines represent the case when the pilot chooses to remain on the ground after engine failure, while in the case of dotted lines the pilot proceeds to climb out of the field. It is interesting to note that in the case of four-engine plane it is safer to continue the flight. The dotted curves also show that the same safety can be achieved with quite a variety of designs.

Payload

Fig. 6 indicates the vast range of payloads possible for constant gross weight. As was to be expected, payload varies directly with the wing loading and inversely with the power loading. It is also worth noting the decrease of the effect of aspect ratio on payload as wing loading goes up.

A large variety of designs will carry identical payloads. For example, 14,000 lbs. payload can be carried either by planes of wing loading of 45 and power loading of 7.9, or by planes of wing loading of 20 and

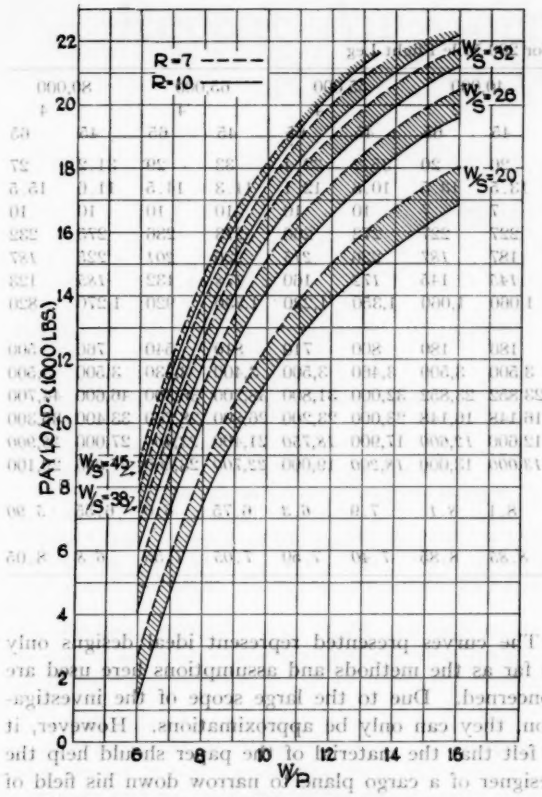

FIG. 6. Payload for 200 mile range.
Gross weight = 55,000 lbs., 65 per cent power.

power loading of 12.2, both of aspect ratio 10. The corresponding cruising speeds are 266 m.p.h. and 203 m.p.h. respectively, at the same 65 per cent power. The former would require an airport length in excess of 3700 ft., while the latter could operate from a 2100 ft. runway.

Similar curves are obtained for cruising at 45 per cent, except that higher payloads are found. The difference tends to vanish as higher power loadings are approached.

Selection of Cargo Plane Design

So far the discussion dealt with some aspects of cargo plane performance. Now all these various findings shall be combined to aid in the selection of the most suitable airplane.

The design characteristics and direct flying costs for each gross weight in turn and cruising at 65 per cent power, are plotted against payload as shown on Fig. 7. The points chosen are those that correspond to the lowest operating cost for each wing loading and yet meet take-off requirements. Examination of the cost curves, particularly for the four-engine craft, illustrates the cost range possible even though only the most economical designs for each wing loading have been selected.

The final selection of the ideal combination is then achieved by drawing the minimum cost envelope. The

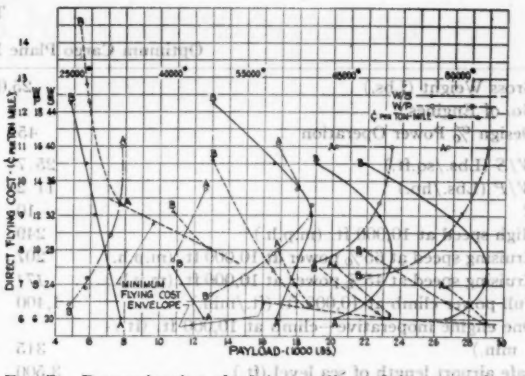

FIG. 7. Determination of minimum direct flying costs for 200-mile flight leg.
100 per cent load factor, 65 per cent power, safe operation from 3500 ft. airport.

plane characteristics can then be read from the curves.

Similar curves can be prepared for cruising at 45 per cent, or any other cruising condition.

Table 1 represents the ideal designs selected in each gross weight class. It is very interesting to note that a plane must be designed specifically for the type of cruising performance selected, if lowest operating cost is to be obtained.

In comparing the four-engine airplanes, it is seen that the larger planes selected for minimum costs are basically slower. This is mainly caused by the fact that uniform airport length was assumed throughout, and the bigger the plane, the bigger is the comparative space required for take-off safety. Wing loading, then, is decreased as gross weight goes up, resulting in slight relative decrease in efficiency.

Fig. 5 showed that take-off plus deceleration runs were critical. The deceleration run increases slightly with size. Also, a more careful propeller and r.p.m. selection may have resulted in higher take-off thrust. As it was, some relative decrease in thrust occurred with increase in size. This, of course, caused the take-off run to increase for the larger planes.

Table 1 illustrates how much more economical it is to operate at 65 per cent power than at 45 per cent. The same point is brought out in Fig. 8, which is a cross plot of data listed in the preceding table. This figure illustrates the decrease of direct flying costs with increase in gross weight. As pointed out before, these results depend to a large extent on the safety criteria and the ratio of cruising power to METO Power.

Such type of presentation enables the designer to pick the most economical design consistent with safety by reading off gross weight, wing and power loadings for a desired payload.

Designing for Minimum Initial Cost

This investigation dealt with aircraft designed, more or less, to the present airline standards. It would be of interest to see what benefit can be derived from designing primarily for the lowest initial cost. For the purposes of illustration, an airplane of 55,000 lbs. gross

TABLE 1

Optimum Cargo Plane Design for 200 Mile Flight Leg

Gross Weight (Lbs.)	25,000		40,000		55,000		65,000		80,000	
No. of Engines	2		2		4		4		4	
Design % Power Operation	45	65	45	65	45	65	45	65	45	65
W/S (Lbs./sq.ft.)	25.7	20	20	20	35.2	32.4	33	29	31.2	27
W/P (Lbs./hp.)	11.2	16	13.5	13.5	10.8	12.1	11.3	14.5	11.6	15.5
R	10	10	7	7	10	10	10	10	10	10
High speed at 10,000 ft. (m.p.h.)	249	207	227	227	272	260	273	236	275	232
Cruising speed at 65% power at 10,000 ft. (m.p.h.)	207	*169*	187	*187*	226	*215*	226	*201*	225	*187*
Cruising speed at 45% power at 10,000 ft. (m.p.h.)	*171*	132	*145*	145	*172*	160	*178*	132	*185*	123
Full power climb at 10,000 ft. (ft./min.)	1,400	898	1,060	1,060	1,350	1,220	1,330	920	1,270	820
One engine inoperative—climb at 10,000 ft. (ft./-min.)	315	190	180	180	800	710	810	540	760	500
Safe airport length of sea level (ft.)	3,500	3,350	3,500	3,500	3,460	3,500	3,400	3,430	3,500	3,500
Weight empty (lbs.)	15,460	14,550	23,852	23,852	32,000	31,800	38,200	36,300	46,600	44,700
Useful load (lbs.)	9,540	10,450	16,148	16,148	23,000	23,200	26,800	28,700	33,400	35,300
Payload for 65% power cruising (lbs.)	6,900	*7,750*	12,600	*12,600*	17,900	*18,750*	21,400	*23,400*	27,000	*28,900*
Payload for 45% power cruising (lbs.)	*7,400*	8,000	*13,000*	13,000	*18,200*	19,000	*22,700*	23,500	*27,000*	29,100
Direct flying cost for 100% L.F. at 65% power (¢/ton-mile)	10.0	*9.3*	8.1	*8.1*	7.9	*6.3*	6.75	*6.0*	6.55	*5.90*
Direct flying cost for 100% L.F. at 45% power (¢/ton-mile)	*9.9*	10.2	*8.85*	8.85	*7.40*	7.50	*7.05*	7.55	*6.8*	8.05

NOTE: Values in italic are those for design power.

weight, 32 lbs./ft.^{2} wing load and 11 lbs./hp. power loading will be considered. The initial cost affects the operating cost through the airplane bare depreciation; while the cost is affected inversely by the cruising speed. Airplane bare depreciation constitutes about 22 per cent of the total operating cost. That means that the above item must be lowered by more than 4.5 per cent for every per cent in speed cost due to sacrifice in design refinement. This presupposes no change in payload, and further assumes that safety performance has not been affected.

CONCLUSIONS

There appears to be nothing basically different in the design of a cargo plane from that of an efficient airliner. However, the speed is important only so far as it affects the operating cost of the plane.

It is hoped that this paper served to emphasize the importance of careful aerodynamic design to obtain a sound economical cargo airplane. At the same time, a method of evaluating the various design factors has been suggested.

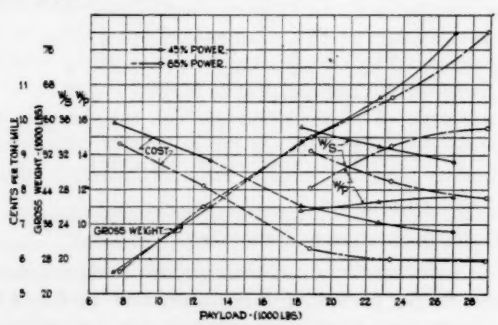

FIG. 8. Variation of gross weight and cost with payload.
200 mile flight leg. Safe take-off from 3500 ft. airport.

The curves presented represent ideal designs only so far as the methods and assumptions here used are concerned. Due to the large scope of the investigation, they can only be approximations. However, it is felt that the material of the paper should help the designer of a cargo plane to narrow down his field of investigation, once the desired payload range has been determined, and to show him what he may expect to find in his studies.

REFERENCES

[1] Jacobs, E. N., Pinkerton, R. M., and Greenberg, Harry, *Tests of Related Forward-Camber Airfoils in the Variable-Density Wind Tunnel*, N.A.C.A., Technical Report No. 610, 1937.

[2] Hood, N. J., *The Effects of Some Common Surface Irregularities on Wing Drag*, N.A.C.A., Technical Note No. 695, 1939.

[3] Stickle, G. W., *Design of N.A.C.A. Cowlings for Radial Air-Cooled Engines*, N.A.C.A., Technical Report No. 662, 1939.

[4] Wood, D. H., *Tests of Nacelle-Propeller Combinations in Various Positions with Reference to Wings. Part I. Thick Wing—N.A.C.A. Cowled Nacelle—Tractor Propeller*, N.A.C.A., Technical Report No. 415, 1932.

[5] Theodorsen, Theodore, Stickle, G. W., and Brevoort, M. J., *Characteristics of Six Propellers Including the High-Speed Range*, N.A.C.A., Technical Report No. 594, 1937.

[6] Douglas, D. W., *The Developments and Reliability of the Modern Multi-Engine Air Liner*, The Journal of the Royal Aeronautical Society, Vol. 39, No. 299, pages 1010–1046, November, 1935.

[7] Johnson, C. L., *Rudder Control Problem of Four-Engined Airplanes*, S.A.E. Journal, Volume 46, No. 6, pages 262–270, June, 1940.

[8] Hartman, E. P., *Considerations of the Take-Off Problem*, N.A.C.A., Technical Note No. 557, 1936.

[9] Wetmore, J. W., *The Transition Phase in the Take-Off of an Airplane*, N.A.C.A., Technical Report No. 626, 1938.

[10] Mentzer, W. C., and Nourse, H. E., *Some Economic Aspects of Transport Airplane Performance*, Part I, Journal of Aeronautical Sciences, Vol. 7, No. 6, pages 227–234, April, 1940.

—, Parts II and III, Journal of Aeronautical Sciences, Vol. 7, No. 7, pages 302–308, May, 1940.

Recent Air Corps Developments in Rotating Wing Aircraft

H. F. GREGORY

U.S. Army Air Corps, Wright Field

ABSTRACT

Introduction. The YG-1B Autogiro was not suitable for needs of Army cooperation because of:

1. Tricky handling characteristics.
2. Insufficient landing and take-off performance.
3. Excess pilot fatigue.
4. Insufficient load carrying capacity.

The recommendations as a result of these tests were:

1. Development of high-performance low-speed airplane.
2. Improved performance of the autogiro.

The Air Corps developed the high-performance low-speed airplane known as the O-49, YO-50 and YO-51. It also carried on developments in the nature of improvements of the YG-1B Autogiro.

Constant Center of Pressure Rotor Blades. The first development was an improved rotor blade having a stable center of pressure tending to eliminate twist and is tapered in planform and thickness.

Accelerated Take-Off Mechanism. The next step was incorporation of an "accelerated take-off mechanism" for varying the angle of pitch of the blades, enabling the pilot to "rev" the rotor in excess of its normal r.p.m. and thereby use the energy stored for an accelerated take-off.

Improved Rotor Starter. An improved rotor starter capable of delivering more power and having an improved clutch arrangement was developed.

Direct Take-Off. The "accelerated take-off mechanism" is now being revised to include a third pitch position of the blade, that position of maximum lift. It is expected that with energy storage by excessive r.p.m. and moving the blade pitch to this position will enable the pilot to take-off directly.

Flexible Pylon Mount. The pylon has been mounted in rubber and is allowed to float, so to speak, thereby improving the vibration characteristics of the craft.

Installation of Larger Engine and Constant-Speed Controllable-Pitch Propeller. A Jacobs 300 horsepower engine and Hamilton Standard constant-speed controllable-pitch propeller are being installed.

Flexible Landing Gear. A highly flexible landing gear, capable of absorbing high loads, is in process of development. Landings from vertical or near vertical descent landings from a 50-foot altitude is expected.

XR-2 Autogiro. All of the above developments are being incorporated in one YG-1B Autogiro, to be redesignated the XR-2.

Feathering Control System. An aerodynamic investigation of a feathering control system is underway. Control of Army autogiros have been effected by tilting of the rotating mass. The feathering control system will vary the pitch of the blade cyclically for control. Ease of control, lessening of pilot fatigue, and improvement of vibration characteristics are expected. The autogiro with this development will be redesignated the XR-3.

Helicopter Development. The Air Corps is engaged in the development of the helicopter. It is reasonable to predict a promising future for this type of craft.

Presented at the Rotating Wing Aircraft session, Ninth Annual Meeting, I.Ae.S., New York, January 29, 1941.

The remarks herein contained are those of the author and are not to be construed as those of the U.S. Army Air Corps.

INTRODUCTION

IN A PAPER presented before the Philadelphia Section of the Institute of Aeronautical Sciences, approximately two years ago, entitled, "Army Experiences with Rotary Wing Aircraft," one of the conclusions drawn was, "Tests now underway indicate that the autogiro may develop into an extremely useful military instrument particularly adapted to certain observation and other needs in Army cooperation." Since that date, the Army did procure seven autogiros and conducted an extended service test with the Cavalry, Field Artillery, Coast Artillery, and Infantry. The results of this extended service test indicated that the actual article undergoing tests was not suitable for their military needs chiefly because of:

1. Tricky handling characteristics.
2. Insufficient performance with reference to landing and take-off characteristics.
3. Excess pilot fatigue in flying.
4. Insufficient load carrying capacity.

The recommendations made as a result of these tests were:

1. In view of the recent development of a high-performance low-speed airplane in a foreign country that the same type of airplane be developed in this country.
2. That the autogiro be developed with special emphasis placed on:
   (*a*) Improving handling characteristics.
   (*b*) Improving take-off and landing characteristics.
   (*c*) Lessening pilot fatigue.
   (*d*) Increasing load carrying capacity.

The Air Corps started the development of the high-performance low-speed airplane which has resulted in the types known to most of you as the O-49, YO-50 and YO-51. It also embarked on the development of the autogiro in an effort to have this type of craft more nearly meet the requirements of the using services. Due to insufficient funds, a decision was made to improve the present type of Army autogiro, thereby reducing costs. Consequently all developments have

been improvements of a nature which could be incorporated in the present Air Corps YG-1B Autogiro. A careful study was made and a program set up for the change, development and test of various items of the service test craft that would eliminate most of the objectionable features and assist in its meeting the requirements for Army cooperation. To eliminate tricky handling characteristics and pilot fatigue, it was necessary to reduce the shaking forces transmitted by the rotor to the control system, the likelihood for any unbalance in the rotor system, and the malfunctioning of the rotor starter transmission.

Constant Center of Pressure Rotor Blades

The first development was an improved rotor blade. In designing this blade, efforts were made to secure a blade having smooth operating characteristics. The blade has an airfoil section having a stable center of pressure, which tends to eliminate twist, and is tapered in planform and thickness from the root to the tip. Tests have indicated that this blade is definitely more smooth than the previous type used on the service test autogiro.

Accelerated Take-Off Mechanism

The next step was the incorporation of a device, commonly called the "accelerated take-off mechanism," for varying the angle of incidence of the blades. With this device the pilot can change the blade angle of incidence, or pitch setting, to either one of two settings, namely, a setting which gives zero lift and consequently minimum drag, or a setting of normal pitch. Friction is controlled in the feathering axis by a clever arrangement of small axial tension members. This device thereby enables the pilot to "rev" the rotor in excess of its normal r.p.m. with the blade at a small angle of incidence until considerable energy has been stored in the rotor. A quick increase in blade angle, therefore, will result in a sudden increase in lift and hence shorten take-off. With this mechanism it is necessary that the craft reach approximately its minimum speed of about 20 miles per hour before changing the pitch setting, thus a short run is required. However, with a wind of approximately 20 miles per hour, it will take off directly.

Improved Rotor Starter

With the "accelerated take-off mechanism," it was necessary to design and build an improved rotor starter transmission, one capable of delivering more power to the rotor and having improved clutch arrangement, eliminating difficulties of the old friction type clutch, such as the "frozen clutch" which can be very embarrassing to the pilot. The new starter also eliminates the necessity of the shear pin in the drive shaft, as it is provided with a device which automatically disengages the clutch when the torque delivered exceeds a predetermined value. To disengage this clutch prior to take-off, it is only necessary to open the throttle.

Direct Take-Off

The "accelerated take-off mechanism" is now being revised to include a third pitch position of the blade, that position of maximum lift. The return from maximum lift position to the normal pitch setting is achieved automatically by the action of centrifugal force on a weight restrained by a spring and interconnected to the blades by a control linkage. Thus the rotor may be allowed to operate as a constant-speed rotor or the pilot may lock the blade in the normal pitch setting. This device has not as yet been tested but it is expected that the autogiro will make a direct take-off in a calm, fully loaded, and without forward roll.

Flexible Pylon Mount

In an effort to reduce vibrations coming into the craft, thereby lessening pilot fatigue and rendering the craft more suitable for missions requiring the use of field glasses or camera, the pylon has been mounted in rubber and is allowed to float, so to speak. This has been tested and there is a marked improvement in the general vibration characteristics of the craft. The vibrations from the rotor are to a great extent absorbed and not transmitted to the fuselage.

Installation of Larger Engine and Constant Speed Controllable Pitch Propeller

In efforts to increase performance and load carrying capacity, the craft has been revised to take an engine of slightly larger horsepower and a constant-speed controlled-pitch propeller. For obvious reasons, the Jacobs L-6MBA engine was selected to replace the Jacobs L-4MA engine installed in the service test craft. The constant-speed controllable-pitch propeller, without question, will lend to greater efficiency and improved performance.

Flexible Landing Gear

To round out the performance of the craft, a highly flexible landing gear capable of absorbing high loads has been designed and is being installed on the craft. While this device has not been tested, it is expected that vertical or near vertical descent landing from a 50-foot altitude can be effected. This landing gear has a travel of approximately 26 inches and is so designed that this travel of the wheels is practically vertical with a negligible horizontal component.

XR-2 Autogiro

All of these developments have been incorporated in one craft. This autogiro has been redesignated as the Army XR-2, and is scheduled for delivery in the early part of the summer of 1941.

Feathering Control System

An aerodynamic investigation of a feathering control system is under way. It was deemed advisable to carry on concurrently a development at a different type of control which shows promise of reducing pilot fatigue and improving general performance. The Army type autogiros were all controlled by tilting the rotating mass. There will be installed a fixed rotor hub and mechanism for varying the angle of incidence cyclically for control on one of the YG-1B type autogiros. The employment of a control system which is not connected to a tilting hub but to the freely flapping blades gives considerable promise. This arrangement varies the angle of attack of the individual blades in such a manner that the normal flapping characteristics are preserved. Obviously, no unbalanced force acting in any direction on the blade can be transmitted to the stick since only the pitch of the blade is defined by the control. As a result, the sole origin of "stick shake" is the angular motion of the blade about its spanwise axis. This angular motion is, of course, produced by the aerodynamic moment characteristics, the mass or inertia moments resulting from the flapping cycle, and the friction in the feathering axis bearing. However, all factors considered, it should be possible to design a feathering system which is smooth in operation. At most, any vibrations in the control system can be confined to those periods when the control stick is actually displaced from neutral. This mechanism will also have a devise for varying the angle of incidence of the blades collectively, thereby permitting an excess r.p.m. and energy storage for a direct take-off. The autogiro with this development will be redesignated the XR-3 and is scheduled for delivery sometime in October.

Helicopter Development

The Air Corps is engaged in the development of the helicopter, details of which have a classified status which prevents elaboration at this time. However, it is reasonable to predict a promising future for this type of rotary wing aircraft.

Institute Notes

S.P.E.E. Annual Meeting

The Forty-Ninth Annual Meeting of the Society for the Promotion of Engineering Education will be held at the University of Michigan, Ann Arbor, Michigan, from Monday, June 23, through Friday, June 27.

Papers will be presented and discussed on the various divisions of engineering education, special subjects and instructional methods. The illustrated Branch Lectures issued by the Institute will be included in the Visual Education Exhibit at the meeting.

Conferences on Aeronautical Engineering will be held on Monday morning, June 23, and Tuesday afternoon, June 24. **Prof. John D. Akerman,** A.F.I.Ae.S., of the University of Minnesota, will be the chairman of these sessions.

Communications to the meeting should be addressed to the General Chairman, S.P.E.E. Convention, 411-A West Engineering Bldg., Ann Arbor, Michigan.

I.Ae.S Student Branch Awards

Last year, the Institute established two annual awards for members of each of the Student Branches—in line with its policy of encouraging and recognizing outstanding accomplishments of young engineers.

The first of these, the "Student Branch Scholastic Award," is presented to a Senior Student Member in each Branch or to a graduate Student Member in each Branch that does not have undergraduate student members, "for attaining the best scholastic record in aeronautical engineering during his Junior and Senior, or Graduate years."

The second award, the "Student Branch Lecture Award," is presented to a Senior or Graduate Student Member in each Branch "for preparing and presenting the best lecture at a regular meeting of the Branch."

As the Journal goes to press, the names of all recipients for this year are not available. An incomplete list follows:

The recipients of the Student Branch Scholastic Award are **Frank E. Bunce,** University of Alabama; **Andrew Smisko,** Boeing School of Aeronautics; **Charles W. Harper,** University of California; **Allen K. Fink,** Carnegie Institute of Technology; **Warren A. Meyer,** Case School of Applied Science; **Irvin Spielberg,** University of Cincinnati; **Leo A. Geyer,** Georgia School of Technology; **Charles W. Burkland,** Iowa State College; **Norman Mayer,** Casey Jones School of Aeronautics; **Malcolm J. Abzug,** Massachusetts Institute of Technology; **Alfred R. Crisi,** New York University; and **J. M. Wright,** Rensselaer Polytechnic Institute.

Those who have received the Student Branch Lecture Award are **Albert C. Grottle,** University of Alabama; **Hollis H. Schuster,** Boeing School of Aeronautics; **Robert J. Grenzeback,** University of California; **Christian G. Weeber,** Carnegie Institute of

Technology; **Wilfred M. Koellish,** Case School of Applied Science; **Hans G. Belitz,** University of Cincinnati; **Andrew A. Mahoff,** Georgia School of Technology; **Robert F. Doudna,** Iowa State College; **Milton F. Edwards,** Casey Jones School of Aeronautics; **Frank B. Kieser,** New York University; and **R. R. Stark,** Rensselaer Polytechnic Institute. The names of other recipients will appear in subsequent issues of the Journal.

Sections

Los Angeles. At a dinner meeting held on May 6, Louis G. Dunn presented a paper on "General Instability Criteria of Stiffened Cylinders." Capt. H. M. McCoy gave a paper on "U.S. Air Corps Propeller Development since 1917" at a previous meeting held on March 11.

San Diego. The first dinner meeting of this Section, held on May 8, was attended by 112 members and friends. Ernest G. Stout of Consolidated Aircraft Corporation gave a paper on "Experimental Determination of Hydrodynamic Stability" which was followed by motion pictures.

Student Branches

Casey Jones School of Aeronautics. Nicholas D. Kintzer presented pins to 45 new members of this Student Branch at a recent meeting. At a previous meeting, Harold B. Fisher spoke on the present activities of the aviation industry.

Louisiana State University. A formal banquet was held on April 30 at which time the following students became members of the Student Branch: Frank Faget, William E. Harding, John Laufer, E. B. Maske, Oliver M. Sokolsky, J. D. Stephenson and Richard H. Truly, Jr.

Massachusetts Institute of Technology. At the last meeting of this semester, held on May 15, the following new officers were elected: Ronald Shainin, Chairman; W. Hoover Shaw, Vice-Chairman; and Charles F. Leiserson, Secretary-Treasurer. Prof. R. H. Smith was re-elected Honorary Chairman.

Rensselaer Polytechnic Institute. Over 1000 people attended a special meeting held on April 24 at which Igor I. Sikorsky was the guest of honor. Mr. Sikorsky spoke on the design and flying characteristics of his helicopter followed by a motion picture film. On May 2, talks by two guests were given: Lt. Comdr. Albert F. Rice, U.S.N., spoke on the life of the flying cadet in the U.S. Navy; and Fred E. Weick spoke on "The Construction of a Fool-Proof Airplane." New officers were elected as follows: George McTigue, Chairman; Warren Tucker, Treasurer; Richard P. Graham, Secretary. Prof. A. J. Fairbanks was re-elected Faculty Advisor.

Personnel Opportunities

The Personnel Bureau serves individual members, as well as organizations seeking to employ aeronautical specialists. Any member or organization may have requirements listed without charge.

Wanted

Through an examination announced some time ago, the Civil Service Commission has been seeking experienced men for procurement inspector positions in the Air Corps of the War Department. The Commission has not been able to obtain enough men for these positions.

Examination No. 6-249 Revised announces open competitive examinations for the positions of **Senior Procurement Inspector,** $2600 a year; **Procurement Inspector,** $2300 a year; **Assistant Procurement Inspector,** $2000 a year; and **Junior Procurement Inspector,** $1620 a year.

The optional branches in which persons may qualify are: Aircraft, Engines, Instruments, Parachutes, Aircraft Propellers, Tools and Gages, Radio, Aircraft Miscellaneous Materials, Textiles, Fur-lined Clothing, and Optical.

Applications may be filed until further notice and may be obtained by writing the Secretary, Board of U.S. Civil Service Examiners, Wright Field, Dayton, Ohio—or at any first or second class post office.

Wanted

Engineering Pilot. Propeller manufacturer has opening in recently organized flight test section for pilot having aeronautical or mechanical engineering training and capable of flying both single and multi-engine types. Address reply to Box 134, Institute of the Aeronautical Sciences.

News of Institute Members

Members are invited to send in news of their activities so that their biographical records may be kept up to date and notices published here for the information of other members.

Paul L. E. Alberti, Technical Member, has left the employ of Lockheed Aircraft Corp. and is now a draftsman with the Vought-Sikorsky Aircraft Division of United Aircraft Corp.

Clarence M. Belinn, M.I.Ae.S., Vice-President of Kansas City Southern Airlines, has been named Director of the Division of Air Transport recently established by the Matson Navigation Company of San Francisco.

At the meeting of the Board of Directors of Republic Aviation Corp. held on May 1, **Ralph S. Damon,** A.F.I.Ae.S., was elected President of the company. He is on indefinite leave of absence from his position as Vice-President in charge of Operations for American Airlines. **W. Wallace Kellett,** President of Republic since 1939, was elected Chairman of its Board of Directors.

The Polytechnic Institute of Brooklyn has created a separate Department of Aeronautical Engineering. The head of the new department is **Dr. R. P. Harrington,** A.F.I.Ae.S., who teaches Theoretical and Applied Aerodynamics and conducts the laboratory courses in connection with the wind tunnel of the Polytechnic Institute. Courses in Aircraft Structures and Aircraft Design are given by **Assistant Professor N. J. Hoff,** M.I.Ae.S.

J. P. H. Hartshorne, M.I.Ae.S., formerly a Ground Engineering Instructor in the British Royal Air Force, is now a Flying Officer in the R.A.F.

P. A. Hewlett, M.I.Ae.S., Vice-President in charge of Sales for Vultee Aircraft, Inc., will be in charge of the company's recently opened office in Washington, D. C.

Murray Kanes, Technical Member, formerly Design Engineer with Republic Aviation Corp., is now on the engineering staff of Goodyear Aircraft Corp.

Philip G. Kraushar, Technical Member, formerly Flight Control Clerk with TWA, is now Senior Meteorologist for Northeast Airlines at Boston Municipal Airport.

Col. G. deFreest Larner, M.I.Ae.S., has taken leave from his position as General Manager of the National Aeronautic Association to go on active duty with the Air Corps. He will serve in London as Assistant Military Attaché for Air at the United States Embassy.

The Reynolds Metals Co. has announced the appointment of **Don A. Luscombe,** A.F.I.Ae.S., as head of the Aircraft Parts Division at its plant in Louisville, Ky. Mr. Luscombe was the organizer of Monocoupe Aircraft Corp. and of the Luscombe Airplane Corp.

Lt. Col. J. T. C. Moore-Brabazon, M.I.Ae.S., F.R.Ae.S., whose appointment as Minister of Aircraft Production was announced by the British Government on May 1, has been a member of the Institute since 1934. His previous office was that of Minister of Transport

Capt. Denis Mulligan, M.I.Ae.S., has been assigned to duty in the Office of the Chief of the Air Corps. He had recently completed a course at the Army Industrial College.

Arthur Nutt, F.I.Ae.S. and Council Member, has been named a member of the Board of Trustees of Worcester Polytechnic Institute. He is Vice-President in charge of Engineering for Wright Aeronautical Corp.

A. M. Rothrock, A.F.I.Ae.S., Senior Physicist in fuel injection and combustion research at the Langley Memorial Aeronautical Laboratories of the N.A.C.A., has been selected by the Society of Automotive Engineers to receive its Horning Memorial Medal for 1940. He will receive the medal for his paper on "A High-Speed Motion Picture Study of Normal Burning, Knock, and Preignition in a Spark-Ignition Engine."

A. Hessell Tiltman, A.F.I.Ae.S., has become a Director of Fireproof Tanks Ltd., as well as Managing Director of Airspeed (1934) Ltd., both of which are British concerns.

Randolph C. Walker, M.I.Ae.S., has relinquished his partnership in the firm of Sutro & Company and assumed the duties of President, General Manager and Chairman of the Board of Aircraft Accessories Corp., Burbank, Calif.

Marvin E. Walseth, Technical Member, has been promoted to the rank of 1st Lieutenant, U.S. Army Air Corps and is now stationed at Ladd Field, Fairbanks, Alaska.

The committee of eleven members recently named to select the recipient of the Collier Trophy for 1941 includes the following Institute members. **Grover Loening** (Chairman), **Major General George H. Brett, Jack Frye, J. H. Kindelberger, Dr. George W. Lewis, Leslie E. Neville** and **William R. Enyart.**

Changes in Membership

The following changes in the membership of the Institute have occurred since the publication of the previous list in the Journal.

Elected to MEMBER Grade

Beauvais, Robert F., Asst. Chief Engineer, Soc. des Moteurs Gnome et Rhone. France.

Bowen, William Harold, M.S. in Ae.E.; Superintendent, Guggenheim Aero. Lab., Calif. Inst. of Technology.

Brownback, Henry Lowe, M.A.; Consulting Engineer (Airplane Engines).

Hartmann, Ernest Christian, M.S. in C.E.; Research Engineer, Aluminum Research Labs., Aluminum Co. of America.

Hoover, Walter Scott, Managing Engineer, in charge Propeller Div., Canadian Car & Foundry Co., Ltd. Canada.

Jenkins, John Gamewell, Ph.D.; Director of Research, Committee on Selection & Training of Aircraft Pilots, National Research Council (see A.M. of S.).

Kintzer, Nicholas Dietrich, Engineering Instructor, Casey Jones School of Aeronautics.

Mendenhall, David Charles, Chief Engineer, Harlow Aircraft Company.

O'Donnell, William Joseph, Ph.D.; Research Engineer, Republic Aviation Corporation.

Pepoon, Philip Waldo, B.S. in M.E.; Jr. Aero. Engineer, Langley Memorial Aero. Lab., N.A.C.A.

Smith, Donald Burdette, Head of Preliminary Design Group, Northrop Aircraft, Inc.

Tuttle, Ralph Moore, Ae.E.; Structures Engineer, Republic Aviation Corp.

Transferred to MEMBER Grade

George Harrison Tweney, B.Ae.E., Instructor in Aeronautical Engineering, University of Detroit; William Mage Smith, Standards Engineer, Bell Aircraft Corp.

Elected to Industrial Member Grade

DuBuque, Jean Howard, Supervisor, Ground School Training, Civilian Pilot Training Service, C.A.A.

Hannah, Charles Cleo, Advertising Surveys, Production Dept., Allison Engineering Co.

Purdy, Charles Van Syclan, Director of Development and Research, The Felters Co., Inc.

Redhed, William Seed, A.B.; Owner, Impact Register Co.

White, Robert Bruce, B.Sc.; Asst. to Vice-President, Transcontinental & Western Air, Inc.

Elected to Technical Member Grade

Atterbury, William Wallace, Jr., B.S.; Student, Harvard Business School.

Davis, George Allen, III, Engineer, Netherlands Purchasing Commission.

Dobkowski, John Chester, Tool and Die Designer, Meyer and Heller Engineering Co.; Aircraft Construction Instructor.

Hage, Robert Evans, M.S.; Instructor in Aero. Engineering, Univ. of Washington.

Heath, Frank Lansing, Inspector, Douglas Aircraft Co.

La Clare, Edward Francis, B.Ae.E.; Pilot, U.S. Army Air Corps.

Larson, Leonard, B.S. in Ae.E.; Northrop Aircraft, Inc.

Martin, Henry Edwin, B.S.; Flight Research Engineer, Douglas Aircraft Co.

Normann, Erik, Jr. Engineer (Instrument Layouts), Cox & Stevens Aircraft Corp.

Petry, Harvey Wayne, Flight Test Engineer, Brewster Aeronautical Corp.

Phillips, William Hewitt, S.M. in Ae.E.; Junior Engineer, Langley Memorial Lab., N.A.C.A.

Simpson, John Walter, B.S. in Ae.E.; Jr. Aero. Engineer, C.A.A.

Sussman, Herman Ralph, M.A.; Shop Work & Instruction, Grumman Aircraft Engineering Corp.; Shop Instructor, Sewanhaka High School, Floral Park, N. Y.

Thomas, William Schoolfield, B.S. in Ae.E.; Jr. Aero. Engineer, C.A.A.

Necrology

Emile Benjamin Wolff

The Institute has recently received notification of the death of Dr. Ir. E. B. Wolff, on February 7, 1941, at Bussum, The Netherlands, after an illness of over a year.

Dr. Wolff was a Fellow of the Institute and one of the group of distinguished foreign aeronautical scientists included among its Founder Members. Born in The Netherlands in 1882, he graduated as a mechanical engineer from the Technische Hoogeschool of Delft in 1904 and received the degree of Doctor of Engineering in 1914. From 1905 to 1918 he was in charge of experimental foundry work and the development of diesel engines for the firm of Werkspoor in Amsterdam. In 1918 he became the Director of the Rijksstudiedienst voor de Luchtvaart. This is the aeronautical research service for The Netherlands, the name of which was changed to Nationaal Luchtvaartlaboratorium in 1937. It was located at the Marine Establishment in Amsterdam until May, 1940, when it was moved to the outskirts of the city. Dr. Wolff had been in active charge of these laboratories continuously until the time of his illness in December, 1939. He resigned as Director in May, 1940.

Technical papers on structures, properties of metal and wood as aircraft construction materials, and aerodynamics, particularly in reference to skin friction and the boundary layer, were among his contributions to the aeronautical sciences.

Dr. Wolff was a Knight of the Order of The Netherlands Lion and a member of the Royal Institute of Engineers of the Hague.

SUGGESTIONS FOR CONTRIBUTORS TO THE JOURNAL *of the* AERONAUTICAL SCIENCES

The Institute of the Aeronautical Sciences invites both members and non-members from any country to submit papers for publication in the Journal of the Aeronautical Sciences. The Journal, following the practice of other scientific publications, does not pay for contributions.

The following directions for the preparation of papers, if followed by authors, will save correspondence, avoid the return of papers for changes, minimize the work of preparation for the printer, and save the expense due to the charges made for "author's corrections."

MANUSCRIPTS: Papers must be written in English, in original typewriting on one side only of white paper sheets, consecutively numbered, and be double or triple spaced with wide margins. Manuscripts should be prepared with great care so that they will be typographically accurate. Paragraphing should be given special attention. Papers should be written in the third person, reference to the writer being made as "the author." Avoid the use of the words "I," "we," and "you." Blueprint copies of papers are unacceptable as it is impossible to mark directions to the printer on them. Correcting, changing, or adding to papers after they are in type is costly. It is, therefore, imperative that papers submitted be in final form. Typographical errors may be corrected on proofs, but if authors wish to add material, they may do so at their own expense. In mailing, drawings may be rolled, but manuscripts should be sent flat. Send by first class mail (register if you wish for your own protection) to the Secretary, Institute of the Aeronautical Sciences, 1505 RCA Bldg. West, Rockefeller Center, New York City. All manuscripts will be examined by the Editorial Committee and by the Editor. Authors will be advised as promptly as possible (usually two to three weeks) whether the paper is acceptable for publication.

TITLES: The title of the paper should be brief. The name and initials of the author should be written as he prefers. The use of the full name of an author is advocated because of the frequent duplication of initials and surnames which sometimes makes it difficult to establish the identity of the author. This is particularly important for large annual indexing and abstracting services. All titles and degrees or honors are omitted. The name of the organization with which the author is associated should be placed after his name on the same line. The date on which the paper is received will be inserted by the Editor.

SUMMARIES OR ABSTRACTS: An abstract to be printed at the beginning should accompany each article. It should be adequate as an *index* and as a *summary*. It should contain a statement of major conclusions reached, since summaries in many cases constitute the only source of information used in compiling scientific reference indexes. Abstracts printed in other journals, especially foreign, in most cases, consist of summaries from printed papers. The summary should explain as adequately as possible the major conclusions to a non-specialist in the subject. The summary should contain from 100 to 300 words, depending on the length of the paper.

SUB-HEADINGS: Sub-headings should be inserted by the author at frequent intervals. The work of editorial preparation will be simplified by the author providing many sub-headings. Owing to the breaking of columns and the insertion of illustrations, some of the sub-headings may have to be omitted.

SHORTENING OF PAPERS: Some papers, at the end, fill in only a portion of a page. This leaves much wasted blank space as succeeding articles are started at the top of a page. Authors should indicate by notation on the left-hand side of the page what matter may be omitted when "run overs" occur. This request is important as the Journal cannot afford in the future, as it has in its earlier issues, to have blank half pages or more at the end of papers.

MATTER USUALLY DELETED: Acknowledgments of assistance in preparation of paper, except by collaborators. Photographs or illustrations of little technical interest and not showing advances in general practice. Too detailed tabular matter (general results of such tables may be included in the text). Lengthy descriptions of materials or processes or of preliminary experiments or theories which preceded final results; salient features only are of interest.

REFERENCES AND FOOTNOTES: References should appear as footnotes only, numbered consecutively, grouped together at the end of the manuscript. The arrangement should be as follows: (for books)—[1] Durand, W. F., *Aerodynamic Theory*, Vol. 1, p. 23; Julius Springer, Berlin, 1934. (For magazines)—Englund, C. R., Crawford, A. B., and Mumford, W. W., *Some Results of a Study of Ultra-Short-Wave Transmission Phenomenon*, Proc. I. R. E., Vol. 20, No. 12, pp. 481 and 482, March, 1933. Please give Author, Title, Volume, page, publisher and date of publication as indicated. Omission of one required fact causes much extra editorial work and possible inaccuracies. All references are grouped at the end of the article.

ILLUSTRATIONS: Illustrations should accompany manuscripts and each should always be referred to in the text, preferably by number. Drawings or graphs should not be larger than 12 × 16 inches, and must be made with jet black India Ink on white paper or tracing cloth, the latter being preferred. *Do not use typewriter for lettering.* The smallest lettering on 8 × 10 inch figures should be no less than 1/4 inch high. Cross-section paper (white with black lines) may be used, but should not have more than 4 lines per inch. If finer ruled paper is used, the major division lines should be drawn in with black ink, omitting the finer divisions. In the case of finely ruled paper, only blue-lined paper can be accepted. *Tracing paper and blueprints* are not acceptable. Lettering and all markings must be large enough to be readable after reduction. Mail rolled or flat, never fold. Drawings which cannot be reproduced (including pencil drawings) will be returned to the author for redrawing, thus delaying publication of the paper. Photographs should be very distinct and show clear black and white contrasts. They must be on glossy white paper. Avoid round and oval photographs.

CAPTIONS AND LEGENDS: Legends or captions must accompany each drawing or photograph submitted. If written on the drawing or photograph, they should be placed below and well outside the part to be reproduced. It is better to place them on separate sheets of paper pasted to the back of the drawings or photographs. Each table should have a caption such as Table 1, Table 2, Table 3, etc. Captions should be complete in themselves so as to make the data intelligible to the reader without reference to the text. A duplicate list of captions for figures should be included as the last page of the manuscript. Use "Fig. 1" (not Figure 1), Figs. 3 and 4, etc., in both the text and the numbering of illustrations. In the text, "Eq. (1)," or "Eqs. (1) and (2)" are preferable to "Equation (1)." In captions and legends, except for "Fig." and "Eq." and table headings, write all words in full; do not abbreviate. Avoid placing explanatory written matter in the drawings; it should be in the text.

MATHEMATICAL WORK: Only the very simplest formulae should be typewritten; all others should be very carefully written in pen and ink, the writing to be large enough so that ample room is provided to mark mathematical matter for the printer. A considerable space for marking should be allowed above and below all equations. All complicated equations should be repeated on separate sheets with plenty of space left for marking. The solidus should be used for simple fractions appearing within the text. Make all expressions clear to the typesetter. Greek letters used in formulae should be clearly designated by name on the margin of the manuscript. All symbols should be clearly written and carefully checked. The difference between capital and lower-case letters should be clearly distinguished and care taken to avoid confusion between zero (0) and the letter (o), between the numeral (one) and the letter (ell) and the prime ('), between alpha and a, kappa and k, u and mu, v and nu, n and eta. All subscripts and exponents should be clearly marked and dots and bars over letters or mathematical expressions should be avoided. Avoid complicated exponents and subscripts. When it is necessary to repeat a complicated expression, it should be represented by some convenient symbol.

NOMENCLATURE AND ABBREVIATIONS: The National Advisory Committee for Aeronautics Nomenclature should be used in preference to any others. Standard abbreviations should be used, and it should be noted that most abbreviations are lower case, such as m.p.h., b.m.e.p., i.hp., b.hp., hp., etc.